



OIST

OKINAWA INSTITUTE OF SCIENCE AND TECHNOLOGY GRADUATE UNIVERSITY
沖縄科学技術大学院大学

The Milstein Bipyridyl PNN Pincer Complex of Ruthenium Becomes a Noyori-Type Catalyst under Reducing Conditions

Author	Louise N. Dawe, Morteza Karimzadeh-Younjali, Zengjin Dai, Eugene Khaskin, Dmitry G. Gusev
journal or publication title	Journal of the American Chemical Society
volume	142
number	46
page range	19510-19522
year	2020-11-09
Publisher	American Chemical Society
Rights	(C) 2020 American Chemical Society This document is the Accepted Manuscript version of a Published Work that appeared in final form in Journal of the American Chemical Society, copyright (C) American Chemical Society after peer review and technical editing by the publisher. To access the final edited and published work see https://pubs.acs.org/doi/10.1021/jacs.0c06518 .
Author's flag	author
URL	http://id.nii.ac.jp/1394/00001651/

doi: info:doi/10.1021/jacs.0c06518

1 The Milstein Bipyridyl PNN Pincer Complex of Ruthenium Becomes a 2 Noyori-Type Catalyst under Reducing Conditions

3 Louise N. Dawe, Morteza Karimzadeh-Younjali, Zengjin Dai, Eugene Khaskin,* and Dmitry G. Gusev*



Cite This: <https://dx.doi.org/10.1021/jacs.0c06518>



Read Online

ACCESS |



Metrics & More

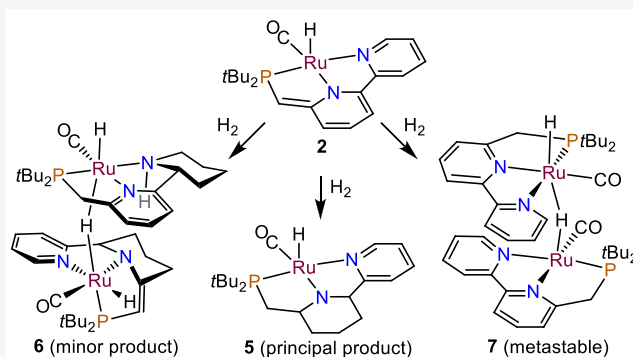


Article Recommendations



Supporting Information

4 **ABSTRACT:** Hydrogenation of the dearomatized PNN ligand of
5 the Milstein bipyridyl complex $\text{RuH}(\text{CO})[\text{PNN}]$ (**2**) gives a
6 square-pyramidal $\text{Ru}(\text{II})$ product $\text{RuH}(\text{CO})[\text{pPNN}]$ (**5**). The
7 central ring of the pPNN ligand is a piperidine. A minor byproduct
8 of the hydrogenation reaction is complex **6** which has a dimeric
9 structure made of two $\text{Ru}(\text{II})$ fragments each possessing a partly
10 hydrogenated PNN ligand. The structures of **5** and **6** have been
11 elucidated by NMR spectroscopy and X-ray crystallography. The
12 PNN ligand of **2** is also hydrogenated under the conditions of the
13 catalytic dehydrogenative coupling of ethanol to ethyl acetate. No
14 direct evidence of the aromatized dihydride $\text{RuH}_2(\text{CO})[\text{PNN}]$ (**4**)
15 was found in this study. However, treating $\text{RuHCl}(\text{CO})[\text{PNN}]$
16 with $\text{Li}[\text{HBET}_3]$ or reacting **2** with H_2 at low temperature resulted
17 in a structurally characterized hydride-bridged dimer (**7**) bearing
18 calculations provided insights into the thermodynamics of the stoichiometric reactions of this work and into the nature of the
19 intermediates of the catalytic ester hydrogenation facilitated by $\text{RuH}_2(\text{CO})[\text{pPN}(\text{H})\text{N}]$ (**8**) formed from **5** under H_2 .

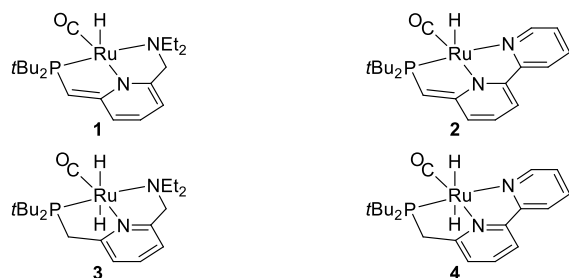


intact aromatized bipyridyl ligands. M06-L/def2-QZVP DFT

20 ■ INTRODUCTION

21 The discovery of the ruthenium complexes **1** and **2** (Scheme
22 **1**)^{1–5} and the concurrent paradigm development of metal–

Scheme 1. Milstein PNN Complexes of Ruthenium



23 ligand cooperation in substrate activation by ligand aromatiza-
24 tion–dearomatization have attracted much attention and
25 discussion in the recent literature.^{6–24} An important reaction
26 of the 16-electron **1** is H_2 addition to give the well-characterized
27 18-electron dihydride **3** of Scheme **1**.^{1,5,25} Surprisingly, no
28 experimental study of **2** has documented the analogous
29 bipyridyl-based PNN dihydride **4**,^{26–43} although this complex
30 featured prominently in the proposed mechanisms of the
31 catalytic reactions of **2**.^{44–49}

32 Herewith, we present a study demonstrating that **4** is an
33 unstable species of which no direct evidence could be obtained

because of a facile H_2 loss resulting in formation of a hydride-
34 bridged dimer. Under reducing conditions, either under H_2 in a
35 hydrocarbon solvent or upon heating in ethanol, the pyridine
36 fragments of the PNN ligand of **2** are hydrogenated. The
37 product compounds are highly active Noyori-type catalysts for
38 ester hydrogenation. A detailed mechanism of the catalytic ester
39 reduction with one of these catalysts is presented, supported by
40 experiment and DFT calculations.

42 ■ EXPERIMENTAL OBSERVATIONS

43 This study started with an attempt to obtain **4** following the
44 procedure reported for **3**.²⁵ Thus, a solution of **2** in a mixture of
45 benzene and hexane (1:1.8 v/v) was pressurized under 50 bar H_2
46 for 4 h. The color changed from the dark green of **2** to dark red-
47 brown; however no product crystallized. This solution was
48 repressured with H_2 and left standing for 3 days. Independently,
49 **2** was reacted with H_2 (50 bar) for 2 h at 100 °C in hexane and in
50 benzene. ³¹P NMR spectra of the product solutions are compiled
51 in Figure 1, and they exhibit several common resonances

Received: June 16, 2020

52 assigned to new complexes **5** and **6**. The details of product
53 isolation and characterization are given below.

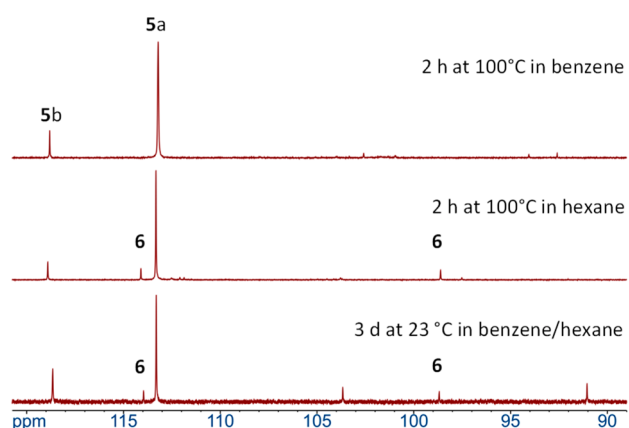


Figure 1. $^{31}\text{P}\{^1\text{H}\}$ NMR spectra of solutions produced by reacting **2** under 50 bar H_2 .

54 Complex **5** was isolated from the benzene reaction solution of
55 **Figure 1**. Evaporation of the solvent, followed by crystallization
56 from hexane at -25°C , afforded an extremely air-sensitive
57 yellow solid (0.18 g, 70% yield). The product is well-soluble in
58 hexane at room temperature, and it is highly soluble in C_6D_6
59 where it exists as a 9:1 mixture of isomers (^{31}P NMR, δ 113
60 (main isomer), 118 (minor isomer)). Slow recrystallization of **5**
61 from hexane at -25°C produced a sample for X-ray analysis that
62 established the distorted square-pyramidal molecular geometry
63 presented in **Figure 2** and assigned to **5a** on the basis of the

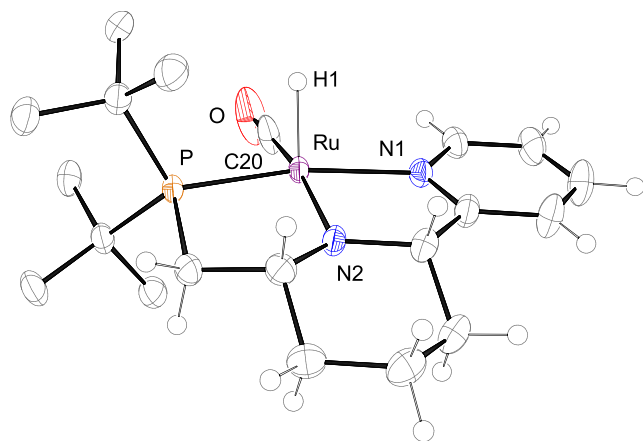


Figure 2. Structure of **5a** with the thermal ellipsoids at 50%. Hydrogens of the *tert*-butyl groups have been removed for clarity. Selected bond distances (\AA) and angles (deg) are the following: Ru–P 2.2706(7), Ru–N1 2.1103(18), Ru–N2 1.9740(19), Ru–C20 1.835(3), Ru–H1 1.51(6), N1–Ru–P 162.99(5), N2–Ru–P 83.93(5), N2–Ru–N1 79.07(7), C20–Ru–P 96.75(7), C20–Ru–N1 99.78(9), C20–Ru–N2 164.57(10), H1–Ru–N2 113(3).

64 NMR data (vide infra). This structure is reminiscent of **2**;
65 however, the central ring of the PNN ligand of **5a** is a piperidine.
66 Overall, **5a** is a formally 16-electron Ru(II) complex where the
67 amido N2–Ru bond is short, 1.974(2) \AA , indicating a double-
68 bond character (a single $\text{N}(\text{sp}^3)$ –Ru bond length is 2.19 \AA on
69 average, when trans to CO, according to the Cambridge
70 Structural Database). The hydrogenated pincer ligand of **5a** will

be further referred to as pPNN; thus the complex is formulated
as $\text{RuH}(\text{CO})[\text{pPNN}]$.

NMR data for the main isomer **5a** are consistent with the
structure of **Figure 2**. The hydride resonance is observed at
 -18.48 ppm, whereas the CH protons of the piperidine
fragment resonate at 3.90 and 3.30 ppm. NOE (nuclear
Overhauser effect) measurements demonstrated a NOE
between the CH protons; their NOEs to the hydride were
also observed, in agreement with their spatial proximity seen in
Figure 2. These experiments further established that the CH at
3.30 ppm is proximal to the PCH₂ protons, whereas the CH at
3.90 ppm is close to the pyridine ring. Complex **5** possesses three
chiral centers (if the piperidine ring is conformationally
nonrigid), and it can exist as a mixture of diastereomers. For
example, isomer **5b** may differ from **5a** by the orientation of the
Ru–H bond with respect to the pPNN ligand plane.

A minor product of the reactions of **Figure 1**, complex **6**,
conveniently crystallized directly from the reaction solutions.
This facilitated the structure characterization by X-ray
crystallography and NMR spectroscopy. The crystals obtained
from the hexane and benzene/hexane solutions of **Figure 1** were
independently analyzed by X-ray diffraction. The complex
structure proved to be the same in both samples. This structure
is presented in **Figure 3** and in **Scheme 2**.

The molecule of **6** is made of two Ru(II) units, each
possessing a hydrogenated PNN ligand, however hydrogenated
in different fragments: in the central ring in one and in the
terminal Py group of the former PNN ligand in the other Ru(II)

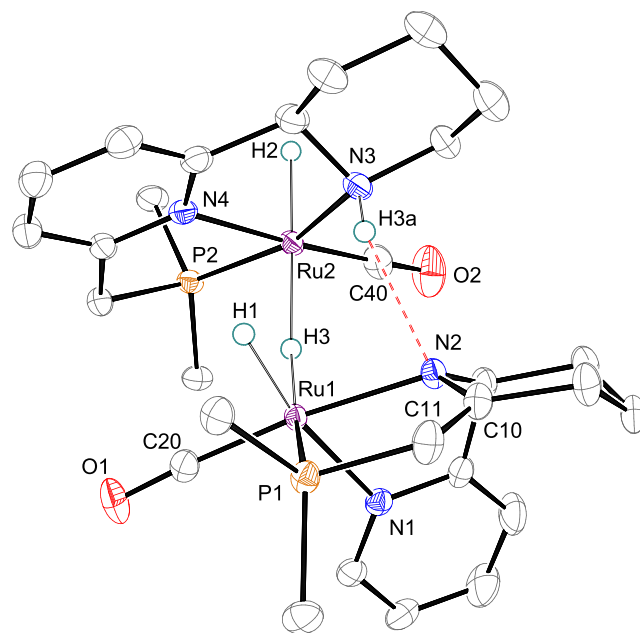
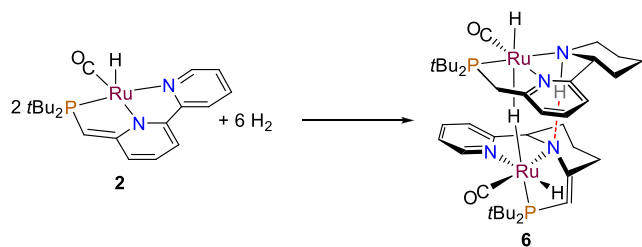


Figure 3. Structure of **6** with the thermal ellipsoids at 50%. The methyl groups and most hydrogen atoms are not shown for clarity. Selected bond distances (\AA) and angles (deg) are the following: Ru1–H1 1.568(17), Ru1–H3 1.76(3), Ru1–P1 2.2996(7), Ru1–N1 2.184(2), Ru1–N2 2.1352(19), Ru1–C20 1.817(2), Ru2–H3 1.81(3), Ru2–H2 1.566(17), Ru2–P2 2.2704(7), Ru2–N4 2.097(2), Ru2–N3 2.172(2), Ru2–C40 1.835(3), P1–C11 1.780(3), C10–C11 1.357(4), C10–N2 1.374(3), N1–Ru1–P1 106.85(5), N2–Ru1–P1 82.00(5), N2–Ru1–N1 75.59(7), C20–Ru1–P1 94.66(8), C20–Ru1–N1 100.82(9), C20–Ru1–N2 174.04(9), N4–Ru2–P2 82.28(6), N4–Ru2–N2 78.00(8), N3–Ru2–P2 160.13(6), C40–Ru2–P2 96.11(8), C40–Ru2–N4 175.64(10), C40–Ru2–N3 103.38(10).

Scheme 2. Formation of the Minor Product, Dimer 6, from Complex 2

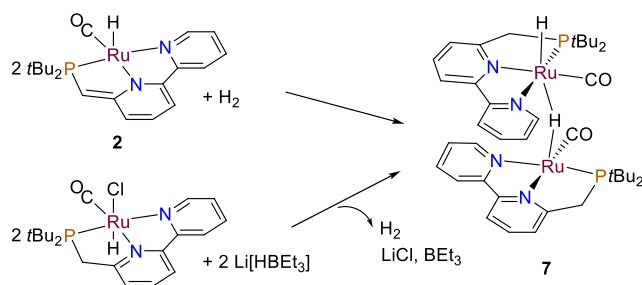


99 unit. Oddly, the C=C bond of dearomatized **2** survived the
100 hydrogenation in one Ru unit, where the hydrogenated PNN
101 ligand adopts an unexpected fac-coordination geometry (note
102 the C10–C11 double bond distance of 1.357(4) Å). The two
103 metal fragments are bridged by a single hydride (H3), and they
104 are further connected by a weak N3–H3a...N2 hydrogen bond
105 (H3a...N2 distance is long, 2.3 Å). The overall structure can be
106 viewed as a product of addition of a 16-electron 5-coordinate
107 amido Ru(II) monohydride (Ru1 fragment) onto an 18-
108 electron octahedral Ru(II) dihydride (Ru2 fragment). The ¹H
109 NMR spectrum of **6** is complicated; however the three hydride
110 resonances are distinct at –10.47 (ddd, *J* = 23.4, 19.0, 5.0 Hz),
111 –12.20 (ddt, *J* = 38.7, 5.9, 5.2 Hz), and –15.72 (dd, *J* = 30.1, 5.1
112 Hz) ppm. The ³¹P NMR spectrum of **6** displays 1:1 peaks at 114
113 and 99 ppm. The unidentified minor species in the bottom
114 spectrum of Figure 1 might be an isomer of **6**.

115 Additional experiments were attempted to produce dihydride
116 **4** in solution. In one, RuHCl(CO)[PNN]³ was treated with
117 ~1.5 equiv of Li[HB(Et)₃] in THF-*d*₈. In two others, **2** was reacted
118 with 1 atm H₂ in methylcyclohexane-*d*₁₄ and in ethyl acetate, in J.
119 Young NMR tubes. The NMR measurements were performed
120 immediately after the sample preparation; particularly, the ethyl
121 acetate solution was kept at –50 to –30 °C except when the tube
122 was vigorously shaken in order to saturate the solvent with H₂.
123 All three experiments cleanly produced deep turquoise solutions
124 of the same product, complex **7**. The NMR spectra were best
125 resolved between –50 and –30 °C; they became very broad at
126 room temperature. Two 1:1 singlets were observed by ³¹P{¹H}
127 NMR at 105 and 123 ppm in THF-*d*₈. Two hydrides of **7** were
128 apparent at –13.40 (ddd, *J* = 2.4, 16.0, 23.7 Hz) and –20.05
129 ppm (ddd, *J* = 4.3, 12.1, 16.0 Hz, in THF-*d*₈) exhibiting a mutual
130 coupling, ²*J*(HH) = 16.0 Hz. Fourteen protons were seen
131 between 5.8 and 7.8 ppm, and four proton resonances of **7**
132 appeared between 2.3 and 3.1 ppm. The NMR data are
133 consistent with the formulation of **7** as a hydride-bridged dimer;
134 the reactions leading to **7** are summarized in Scheme 3.

135 Complex **7** crystallized from the ethyl acetate solution upon
136 standing overnight at room temperature, and the product

Scheme 3. Formation of Dimer 7



structure of Scheme 3 was confirmed by X-ray crystallography 137
(Figure 4). Dimer 7 can be viewed as an adduct of **4** with the 138 44

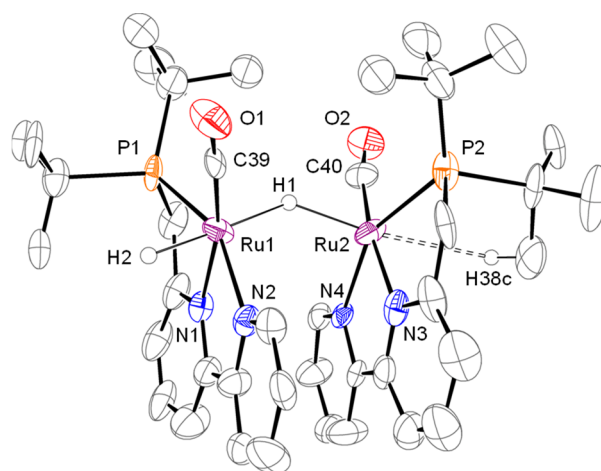


Figure 4. Structure of **7** with the thermal ellipsoids at 50%. Most hydrogen atoms are not shown for clarity. Selected bond distances (Å) and angles (deg) are the following: Ru1–H1 1.82(3), Ru1–H2 1.54(3), Ru1–P1 2.275(4), Ru1–N1 2.077(11), Ru1–N2 2.058(11), Ru1–C39 1.829(13), Ru2–H1 1.81(3), Ru2–P2 2.266(4), Ru2–N3 2.061(11), Ru2–N4 2.100(10), Ru2–C40 1.843(13), Ru2–H38c 2.67, N1–Ru1–P1 82.0(3), N2–Ru1–P1 153.0(4), N2–Ru1–N1 76.3(4), C39–Ru1–P1 95.8(4), C39–Ru1–N1 167.7(5), C39–Ru1–N2 102.0(5), N3–Ru2–P2 81.7(4), N3–Ru2–N4 78.4(4), N4–Ru2–P2 152.2(3), C40–Ru2–P2 98.0(5), C40–Ru2–N3 168.4(5), C40–Ru2–N4 97.6(5).

four-coordinate 16-electron *d*⁸-Ru⁽⁰⁾(CO)[PNN]. The two 139
metal fragments appear to be held together by a bridging 140
hydride. The Ru–H1 distances are similar in Figure 4; however
when optimized by DFT (vide infra), the structure develops a 142
short Ru2–H1 (1.67 Å) bond and a long Ru1–H1 (2.14 Å) 143
distance. This computational result agrees with the observation 144
of unequal couplings: ²*J*(H1–P2) = 12.1 Hz and ²*J*(H1–P1) = 145
4.3 Hz. The crystallographic Ru1–Ru2 distance in **7** is 3.39 Å, 146
and it is considerably shorter than the sum of the van der Waals 147
radii, 4.1 Å, thus suggesting some metal–metal bonding. Metal 148
oxidation states are ambiguous in this structure; e.g., one can 149
view **7** as composed of two Ru^(I)H(CO)[PNN] fragments. A 150
possibly very weak agostic interaction of Ru2 with the C38– 151
H38c bond is present in **7**; however the Ru2–H38c distance is 152
long, 2.67 Å. 153

Complex **7** is not stable under H₂ in hydrocarbon solvents, 154
and significant changes occur already in 2 h at room temperature 155
in C₆D₆, illustrated in Figure 5 (bottom trace). The hydride 156 65
resonances of **7** are seen there as the very broad lines near –13 157
and –20 ppm. Both isolated products, the major (**5**) and the 158
minor (**6**), are apparently present in solution, and it seems that 159
they are formed independently. Four sharp doublets seen 160
between –19 and –25 ppm can be tentatively assigned to the 161
intermediates (possibly diastereomers) formed by addition of 162
one or two H₂ molecules to the PNN ligand of **2**. 163

Through the rest of this section, we report on some reactivity 164
of complexes **2** and **5**. It might be already apparent from the 165
spectra of Figure 1 that **5** does not form an isolable dihydride 166
RuH₂(CO)[pPN(H)N] (**8**) as in Scheme 4. To probe whether 167 84
dihydride **8** could be observable in solution, we prepared a 168
sample of **5** in C₆D₆, under 1 atm H₂. The recorded ¹H NMR 169
spectrum was virtually indistinguishable from that of **5** under Ar. 170

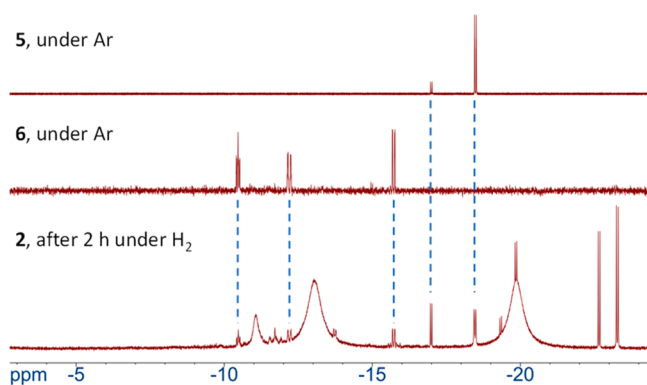
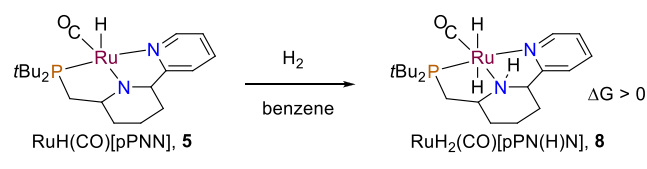


Figure 5. Hydride region of the ^1H NMR spectra of C_6D_6 solutions of **5** and **6** under Ar and **2** under 1 atm H_2 at 23 $^\circ\text{C}$.

Scheme 4. Formation of Dihydride **8**



171 A signal of the dissolved H_2 was observed, indicating that
172 formation of **8** is thermodynamically unfavorable.

173 Complex **5** reacts with ethanol at room temperature to give
174 two species. In neat ethanol- d_6 , these are in an approximately 10:1
175 ratio in the ^{31}P NMR spectrum at 98.5 and 100 ppm,
176 respectively. The NMR spectra of the product, presumed to
177 be the ethoxide $\text{RuH}(\text{OEt})(\text{CO})[\text{pPN}(\text{H})\text{N}]$ (**9**), are well-
178 defined, although the hydride site is 95% deuterated in ethanol-
179 d_6 ; the residual RuH is observable at -16.68 ppm (d , $J(\text{HP}) = 26$
180 Hz). A slow H/D exchange also occurs in **9** in one piperidine
181 CH group, at 3.98 ppm. The d_5 -ethoxide ligand of **9** was not
182 observed in the ^{13}C NMR spectrum, presumably because of a
183 rapid exchange with the solvent.

184 To compare the complexes of this work in catalytic
185 hydrogenation, we tested them in the reduction of ethyl acetate
186 (EA) and methyl hexanoate (MH). The results are compiled in
187 Table 1. Under the solventless base-free conditions, complexes **5**
188 and **6** proved to be highly efficient for the reduction of the esters
189 to give the corresponding alcohols: ethanol, hexanol, and
190 methanol. This is not too surprising in the case of **5** since the

Table 1. Catalytic Reduction of Ethyl Acetate (EA) and Methyl Hexanoate (MH)^a

line	cat. ^b	ester ^c	% conv ^d	TON ^e
1	2	EA	18.0	1960
2	2	MH	23.5	2500
3	3	EA	2.4	240
4	3	MH	6.5	648
5	5	EA	89.5	8625
6	5	EA	31.5	630 ^f
7	5	MH	61.2	6123
8	6	EA	97.8	9776
9	6	MH	91.7	8964

^a3 h at 100 $^\circ\text{C}$, initial $p(\text{H}_2) = 50$ bar, in a 300 mL Parr reactor magnetically stirred at 500 rpm. ^bCatalyst, 2×10^{-5} mol. ^cSubstrate, 0.2 mol. ^dPercent conversion of ester to alcohol. ^eEster to alcohol turnover number. ^fAt 25 $^\circ\text{C}$, $S/C = 2000$.

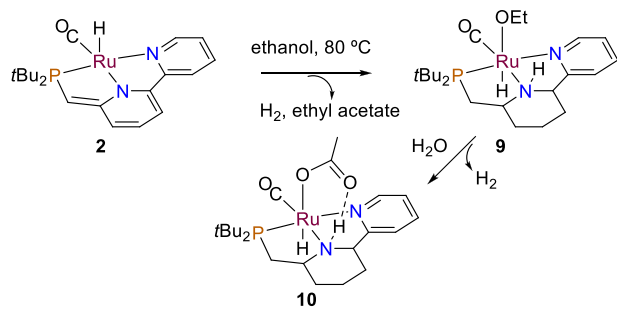
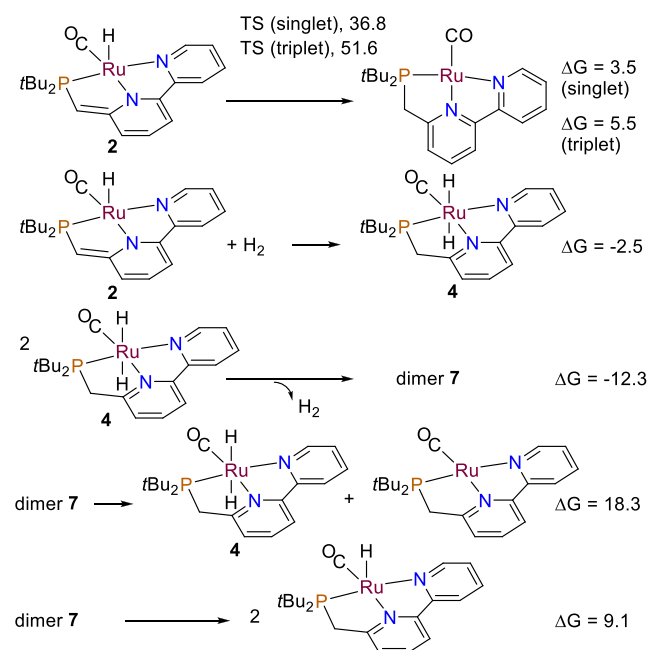
complex is closely related to several existing PNN hydro-
191 generation catalysts of ruthenium and osmium.^{50–55} Complex **5** is
192 active for the reduction of ethyl acetate even at room
193 temperature, affording TON = 630 in 3 h. The Milstein catalyst
194 **3** was markedly less efficient under the reaction conditions of
195 Table 1, although these may not be optimal with **3**. For instance,
196 the catalytic efficiency of **3** toward EA was shown to be
197 significantly better under basic conditions.²⁵ 198

The dearomatized **2** exhibited good catalytic activity toward
199 the reduction of EA and MH, yet distinctly lower than that of **5**
200 or **6**. The reduction of the PNN ligand of **2**, which was facile in
201 the hydrocarbon solvents, might be somewhat retarded in an
202 ester media. This idea is partly supported by the observation that
203 complex **7** (formed from **2** under H_2) was relatively stable in and
204 crystallized from ethyl acetate, under H_2 . When a solution of 20
205 mg of **7** in ethyl acetate, sealed in a J. Young NMR tube under 1
206 atm H_2 (H_2/Ru molar ratio of ~ 2.5), was heated at 80 $^\circ\text{C}$ for 2 h,
207 the dimer persisted in solution and accounted for 64% of the
208 total ^{31}P integral signal intensity. An estimated 2–3 equiv of
209 ethanol was produced during this time, indicating that
210 practically all hydrogen was consumed and that transfer of
211 hydrogen from **7** to ethyl acetate was slow even at 80 $^\circ\text{C}$.
212 Formation of a new ruthenium hydride complex was observed in
213 this solution (d , $\delta = -17.07$, $^2J(\text{H}-\text{P}) = 26.3$ Hz, (see Figure S30
214 for details). 215

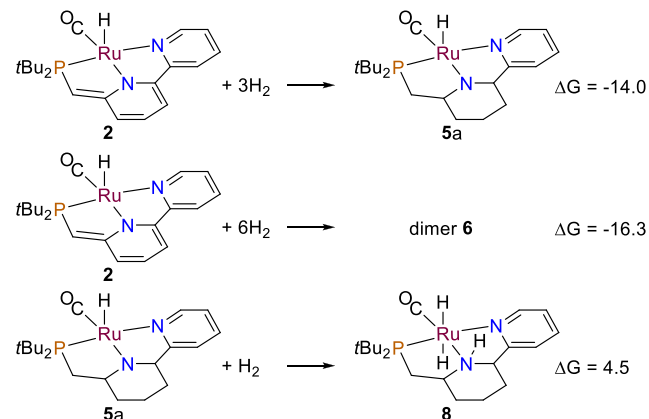
Recently, Chianese published a reaction of **1** with PCy_3
216 in toluene at 100 $^\circ\text{C}$ that gave a Ru(0) imine product.⁵⁶ Under H_2 ,
217 the imine was converted into a Noyori-type catalyst that proved
218 to be competent for ester hydrogenation. We briefly checked
219 whether the Milstein catalyst complex **3** is stable at 100 $^\circ\text{C}$ under
220 50 bar H_2 . Two experiments in benzene, with heating for 2 and 4
221 h, respectively, gave similar results. Two peaks dominated the
222 ^{31}P NMR spectra of the product solutions, at 124 and 117 ppm,
223 contributing approximately 20% and 55% to the total ^{31}P signal
224 integration, respectively, after 4 h of heating. The former
225 chemical shift corresponds to **3**, whose hydrides were observed
226 at -4.18 ppm. The latter is an unknown species, associated with
227 three hydride resonances at -7.54 (t , $J(\text{HP}) = 7.2$ Hz), -9.61 (t ,
228 $J(\text{HP}) = 54.5$ Hz), and -10.65 (non-first-order m), in a 1:1:2
229 ratio. Further studies of the product (evaporated and redissolved
230 in C_6D_6) identified the resonances of the pyridine protons (δ
231 8.01 (d), 7.16 (t), and 6.71 (d)) and those of the diastereotopic
232 protons of the CH_2 groups (δ 5.05 (d), 4.68 (d), 3.49 (dd) and
233 3.13 (dd)), each of these integrated as 2H vs the hydrides. The
234 NCH_2 resonance of the ethyl groups appeared at 2.79 ppm as a
235 quartet of integration 8H. The NMR data indicate a dimeric
236 structure possessing an intriguing symmetry but do not allow a
237 reliable structural assignment. Nevertheless, these experiments
238 confirmed that **3** persists upon heating under H_2 at 100 $^\circ\text{C}$, and
239 the two principal species in solution possess an intact 2-
240 $(\text{CH}_2\text{PtBu}_2)$ -6- $(\text{CH}_2\text{NEt}_2)$ - $\text{C}_6\text{H}_3\text{N}$ ligand on ruthenium. 241

In the final experiment, we pursued the question of whether
242 the PNN ligand of complex **2** might undergo hydrogenation
243 under the conditions of the catalytic acceptorless alcohol
244 dehydrogenation. This was probed by heating a solution of **2** in
245 ethanol (0.067 M) at 80 $^\circ\text{C}$ in a J. Young NMR tube vented
246 through the top via a piece of tubing connected with a bubbler.
247 NMR spectra were recorded after 2 and 6 h of heating; these
248 spectra exhibited only minor differences. The principal product
249 was observed at 100 ppm in the $^{31}\text{P}\{^1\text{H}\}$ NMR; the integration
250 of this peak changed from 81% (2 h) to 88% of the total ^{31}P
251 NMR signal after 6 h of heating. The hydride resonance of the
252 product appeared at -17.54 ppm (d , $J = 26.4$ Hz). Formation of 253

254 ethyl acetate was evident from the spectra; the TON (turnover
 255 number) of ethanol to ethyl acetate of 26 and 34 was recorded in
 256 2 and 6 h, respectively. The ^1H and $^{13}\text{C}\{^1\text{H}\}$ NMR shifts of the
 257 pincer ligand of the main product closely match those of the
 258 ethoxide **9**. Thus, the NMR observations unambiguously
 259 confirm that the PNN ligand of **2** is hydrogenated under the
 260 conditions of the dehydrogenative coupling of ethanol. When
 261 analyzing the ^{13}C NMR spectrum (Figure S16), we noticed two
 262 peaks at 181.9 and 25.4 ppm, the shifts being similar to those of
 263 the acetate ligand of $\text{RuH}(\text{OAc})(\text{CO})[\text{HN}(\text{CH}_2\text{CH}_2\text{P}i\text{Pr}_2)_2]$
 264 (181.4 and 26.1 ppm) reported by Gauvin and co-workers.⁵⁷
 265 The acetate could form as a result of the dehydrogenative
 266 coupling of ethanol with a trace amount of water in the solvent;
 267 this chemistry is well-documented.⁵⁷ It is reasonable to postulate
 268 that **9** might form during the reaction of **2** with ethanol,
 269 according to Scheme 5; however the more stable acetate
 270 complex **10** is the thermodynamic product in ethanol containing
 271 adventitious water.

Scheme 5. Reduction of **2** in EthanolScheme 6. Calculated Reaction Gibbs Energies of the Stoichiometric Transformations of **2**, **4**, and Dimer **7**^a

^aCalculated in benzene solvent continuum (all 1 M solutes, at 298.15 K, $p(\text{H}_2) = 1$ atm). The energies of the reactions of **7** are per mole of the dimer formed or reacted.

Scheme 7. Calculated Reaction Gibbs Energies for **2** and **5a** with H_2 ^a

^aCalculated in benzene solvent continuum (all 1 M solutes, at 298.15 K, $p(\text{H}_2) = 1$ atm). Mass balance is ensured throughout.

272 DFT COMPUTATIONAL DATA

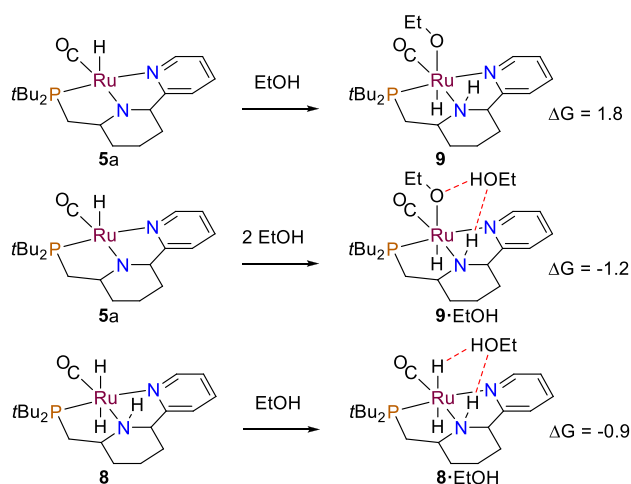
273 Reactions of the complexes of this work were investigated with
 274 the help of M06-L/def2-QZVP DFT calculations. We shall first
 275 look at the stoichiometric transformations of **2**, **4**, and dimer **7** in
 276 benzene, summarized in Scheme 6. Isomerization of **2**, leading
 277 to the square-planar $\text{Ru}^{(0)}(\text{CO})[\text{PNN}]$ species is unfavorable,
 278 yet the product singlet structure is only marginally less stable.
 279 Considering the reaction barrier of 36.8 kcal/mol from **2**, the
 280 isomerization is expected to be slow at room temperature.

281 Formation of **4** from **2** under 1 atm H_2 is a favorable process.
 282 Therefore, the reason why **4** has not been observed must be due
 283 to relatively fast dimerization leading to **7**. Indeed, the formation
 284 of the dimer is exergonic by -12.3 kcal/mol. Considering the
 285 dissociation reactions of **7** of Scheme 6, it is clear that the release
 286 of **4** back (together with $\text{Ru}(\text{CO})[\text{PNN}]$) is unlikely, being 18.3
 287 kcal/mol uphill. It is however possible that **7** can split to give a
 288 trace of the paramagnetic 17-electron species $\text{Ru}^{(1)}\text{H}(\text{CO})$ -
 289 $[\text{PNN}]$.

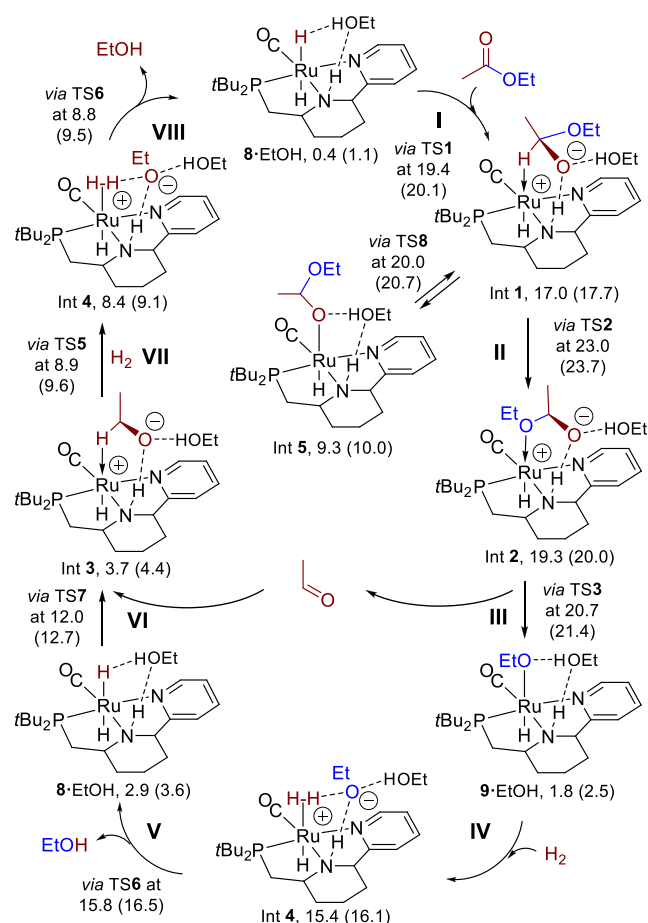
290 Formation of the isolated products **5a** and **6** in Scheme 7 is
 291 accompanied by the relatively large Gibbs energies of -14.0 and
 292 -16.3 kcal, respectively, per mole of **2** reacted. Finally,
 293 formation of dihydride **8** is indeed thermodynamically
 294 unfavorable, in agreement with the experimental observations.

295 In Scheme 8, we are looking at the energies of ethanol
 296 addition to **5a** and hydrogen bonding of ethanol with **8** and **9**.
 297 Formation of ethoxide **9** is an endergonic process; however the
 298 product is stabilized by hydrogen bonding with ethanol in **9**.
 299 EtOH . We should treat **9**· EtOH as a minimal model of this
 300 species. Similarly, **8** can favorably bind a molecule of EtOH .

301 Next, a plausible mechanism of the catalytic reduction of ethyl
 302 acetate to ethanol with **5a** under $p(\text{H}_2) = 50$ atm was calculated,
 303 following the ideas of others and those of our own.^{22,25,53,57-65}
 304 The results are organized in the form of the catalytic cycle of
 305 Scheme 9. Two sets of energies are given there. The first is vs **5a**;
 306 e.g., the entry into the catalytic cycle, **8**· EtOH , is at 0.4 kcal/mol.
 307 The second set of energies (given in parentheses) is vs **9**· EtOH ,
 308 and then **8**· EtOH is at 1.1 kcal/mol. The systematic difference
 309 between the two energy sets is negligible, 0.7 kcal/mol.
 310 Nevertheless, it is important to recognize that once the catalytic
 311 reaction has generated enough alcohol, the most stable
 312 ruthenium species in solution is **9**· EtOH . All structures of

Scheme 8. Calculated Reaction Gibbs Energies for **5a** and **8** with EtOH^a

^aCalculated in benzene solvent continuum (all 1 M solutes, at 298.15 K).

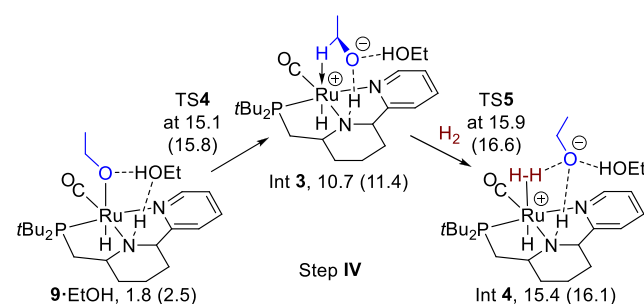
Scheme 9. Catalytic Hydrogenation of Ethyl Acetate with **8**^a

^aM06-L/def2-QZVP Gibbs energies (kcal/mol) of the species in ethyl acetate solvent continuum (all 1 M solutes, at 298.15 K, under 50 atm H₂) vs **5a** + EtOH + H₂, or (in parentheses) vs **9**·EtOH + H₂. Mass balance is ensured throughout.

The hydrogenation starts by a hydride transfer to ethyl acetate 315 in step I. With TS1 at 19.4 (20.1) kcal/mol, this should be facile. 316 The product zwitterionic 1-ethoxyethoxide complex Int 1 may 317 rearrange to give Int 5; however the productive pathway from 318 Int 1 is step II, to Int 2. It is this step that encounters the largest 319 barrier in the catalytic cycle, TS2 at 23.0 (23.7) kcal/mol. The 320 height of this barrier agrees with the observation that the 321 reduction of ethyl acetate with **5** was relatively fast at 25 °C 322 (Table 1, line 6). Elimination of acetaldehyde from Int 2 in step 323 III is practically barrierless; this gives the ethoxide **9**·EtOH. 324

Step IV of Scheme 9 proved challenging to calculate. Two 325 plausible scenarios of the ethoxide substitution by H₂ were 326 investigated: unimolecular S₁ and bimolecular S₂. The S₁ process 327 starts by elimination of the ethoxide to give a 16-electron 328 cationic ruthenium intermediate that subsequently adds H₂. S₂ is 329 a bimolecular reaction where the ethoxide is displaced by H₂. 330 Attempts to find the corresponding transition states have been 331 unsuccessful. What became apparent when working on the S₁ 332 process was the tendency of the ethoxide, upon elimination, 333 to rearrange into an agostic species Int 3 via TS4, as shown in 334 Scheme 10. Then, the agostic ethoxide can be displaced by H₂ 335 via TS5, affording the dihydrogen complex Int 4. 336

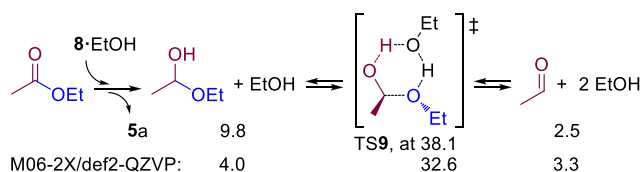
Scheme 10. Composite Step IV



The rest of the catalytic cycle is straightforward. Deprotona- 337 tion of the H₂ ligand of Int 4 in step V of Scheme 9 is facile. This 338 regenerates the catalyst **8**·EtOH, followed by insertion of the 339 aldehyde intermediate in step VI. The product, agostic ethoxide 340 Int 3, undergoes substitution with H₂ in step VII. The catalyst **8**· 341 EtOH is regenerated once again after deprotonation of the 342 dihydrogen ligand of Int 4 in step VIII. The overall process, 343 EtOAc + 2H₂ (50 atm) → 2EtOH, is accompanied by ΔG = 344 -4.5 kcal/mol. A perhaps more accurate energy of this organic 345 reaction is ΔG = -7.2 kcal/mol, calculated using the M06-2X/ 346 def2-QZVP method which is better suited for main-group 347 thermochemistry than M06-L/def2-QZVP that we prefer for 348 organometallic reactions of transition metal complexes. 349

The events of Scheme 9 do not involve the conventional 350 metal–ligand cooperation (MLC) often associated with the 351 Noyori-type catalysts.²² MLC ideas envisage that “the non- 352 innocent ligands directly participate in the substrate activation 353 and in the bond formation” in the metal–ligand cooperating 354 bifunctional catalysts.⁶⁸ Thus, a mechanism was considered here 355 where the transfer of a metal hydride and the NH proton of **8**· 356 EtOH to ethyl acetate gave 1-ethoxyethanol according to 357 Scheme 11. The energy of this reaction, EtOAc + **8**·EtOH → 1- 358 ethoxyethanol + **5a** + EtOH, is the energy of hydrogenation of 359 ethyl acetate: EtOAc + H₂ (50 bar) → 1-ethoxyethanol, when **8**· 360 EtOH is referenced to **5a** + EtOH + H₂ (50 atm) as in Scheme 9. 361 This organic reaction energy was calculated to be 9.8 and 4.0 362 kcal/mol with the M06-L/def2-QZVP and M06-2X/def2- 363

313 Scheme 9 were optimized in ethyl acetate solvent continuum; 314 thus, the ester is both the solvent and the substrate.

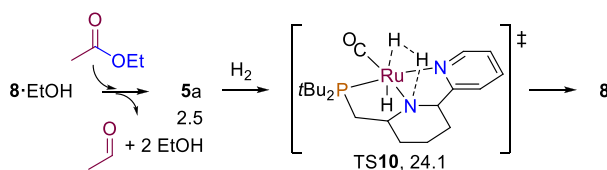
Scheme 11. Formation and Splitting of 1-Ethoxyethanol^a

^aThe reaction Gibbs energies (kcal/mol) are in ethyl acetate solvent continuum (all 1 M solutes, at 298.15 K). Mass balance is ensured throughout.

364 QZVP methods, respectively, the latter value being presumably
365 more accurate.

366 1-Ethoxyethanol can split into acetaldehyde and ethanol in
367 solution. A slow equilibrium between these species was indeed
368 observed by solution NMR spectroscopy, and the reaction
369 energy of 0.3 kcal/mol was estimated from the equilibrium
370 constant in ethanol, at room temperature.⁵¹ The M06-2X/def2-
371 QZVP value of $\Delta G = 3.3 - 4.0 = -0.7$ kcal/mol calculated in
372 ethyl acetate is reasonably consistent with the experiment. As is
373 apparent from Scheme 11, transition state TS9 for the ethanol-
374 assisted C–O bond cleavage of 1-ethoxyethanol is at 32.6 kcal/
375 mol (M06-2X/def2-QZVP energy), and this process is
376 unfavorable considering the much lower barrier TS2, 23.0
377 kcal/mol, in step II of Scheme 10. While the formation of 1-
378 ethoxyethanol is not precluded, this and the organic reaction of
379 Scheme 11 via TS9 seem catalytically irrelevant.

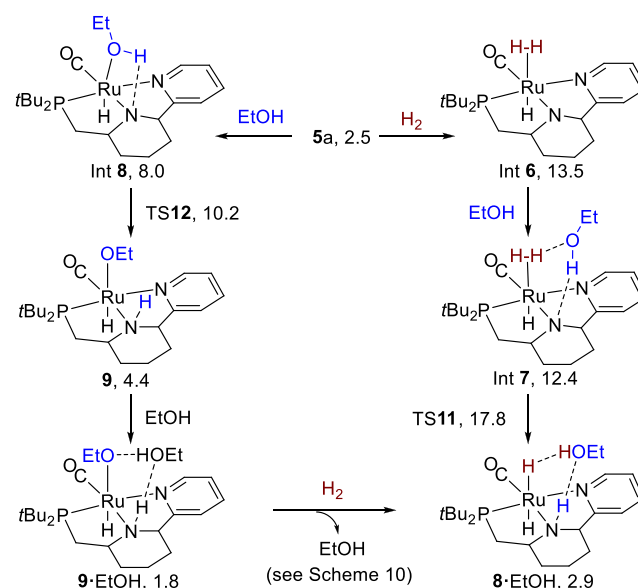
380 We also calculated barrier TS10 for H₂ addition to complex
381 5a. TS10 is at 21.5 kcal/mol vs 5a and H₂ (50 atm). When 5a
382 originates from 8·EtOH and ethyl acetate according to Scheme
383 12, then 5a is at 2.5 kcal/mol and TS10 is at 24.1 kcal/mol. This

Scheme 12. H₂ Addition to Complex 5a^a

^aM06-L/def2-QZVP Gibbs energies (kcal/mol) of the species in ethyl acetate solvent continuum (all 1 M solutes, at 298.15 K, under 50 atm H₂) vs 5a + EtOH + H₂. Mass balance is ensured throughout.

384 barrier is too high (vs TS5 at 15.9 kcal/mol) for the reaction to
385 proceed via the conventional MLC mechanism. The ethoxide
386 substitution by H₂, illustrated in Scheme 10, is a lower energy
387 process for the regeneration of the dihydride catalyst. It is, of
388 course, counterintuitive that H₂ addition to the five-coordinate
389 complex 5a should be a higher-energy process compared to the
390 same reaction of the octahedral complex 9·EtOH.

391 A further argument could be made that the H₂ splitting on 5a
392 might be facilitated by ethanol via Int 7 and TS11 of Scheme 13.
393 The energy of TS11 is indeed lower than that of TS10, 17.8 vs
394 24.1 kcal/mol. However, the ethanol competes with H₂ in the
395 reaction with 5a. Ethanol addition to 5a gives Int 8, then
396 ethoxide 9 via TS12. When enough ethanol is present, complex
397 9·EtOH will be formed, the overall reaction 5a + 2EtOH → 9·
398 EtOH being an exergonic process, as was already noted in
399 Scheme 8. The energy differences between the two competing
400 pathways of Scheme 13 favor ethanol addition to 5a when
401 [EtOH] ≥ [H₂]. The mole fraction solubility of H₂ in ethyl

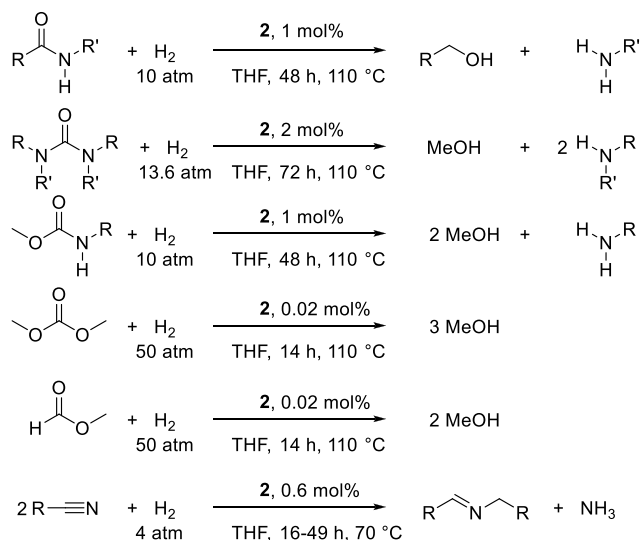
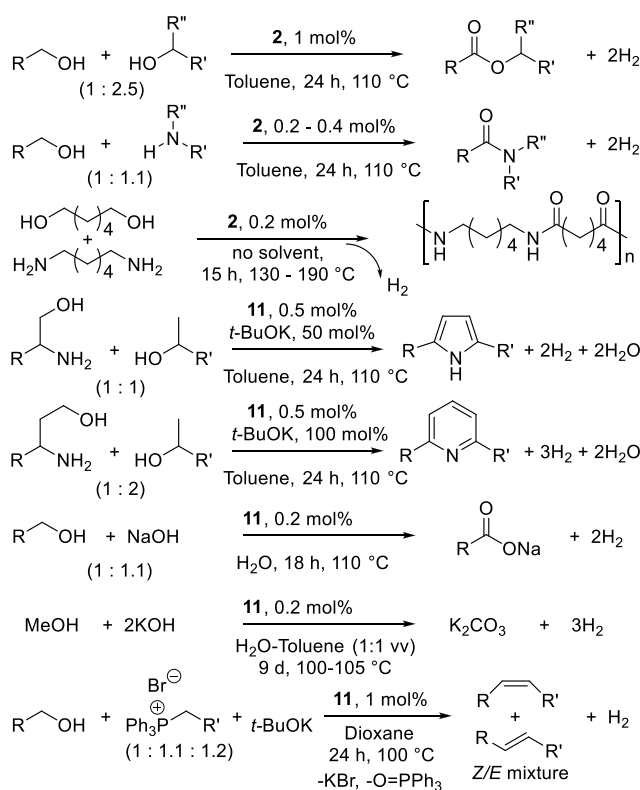
Scheme 13. H₂ vs EtOH Addition to 5a^a

^aM06-L/def2-QZVP Gibbs energies (kcal/mol) of the species in ethyl acetate solvent continuum (all 1 M solutes, at 298.15 K, under 50 atm H₂) vs EtOAc + 5a + EtOH + H₂. Mass balance is ensured throughout.

acetate is $\sim 3.5 \times 10^{-4}$ under 1 atm H₂ at 298 K.⁶⁹ When EtOAc/ 402
5a ratio is 10⁴ (the S/C ratio in Table 1), the corresponding H₂/ 403
5a ratio is ~ 3.5 . This ratio will increase with increased *p*(H₂) and 404
temperature; nevertheless, when ethyl acetate conversion to 405
ethanol would reach 1% (TON = 100, or 200 equiv of alcohol 406
produced), the likelihood of formation of the dihydrogen 407
complex Int 6 from 5a (if the latter is present) should become 408
negligible, and the proton shuttle pathway of Scheme 13 can be 409
safely ignored as a mechanism of the dihydride catalyst 410
regeneration. Through most of the catalytic reaction, the 411
catalyst 8·EtOH originates from 9·EtOH via Int 3, as illustrated 412
in Schemes 9 and 10. 413

DISCUSSION

414
Complex 2 has been used in a large variety of catalytic reactions. 415
Hydrogenations of amides, urea derivatives, carbamates, 416
carbonates, esters, and nitriles with 2 have been reported, 417
summarized in Scheme 14.^{3–5,26,29,30,38,40} Rearomatization of 418 s14
the PNN ligand of 2 and formation of a dihydride intermediate 419
under H₂ were suggested in the proposed mechanisms.^{3,5,30} 420
Dehydrogenative coupling reactions of alcohols have also been 421
successful with 2. The precursor to 2, RuHCl(CO)[PNN] 422
(11),³ could also be used, in combination with a base. These 423
catalytic reactions included cross-dehydrogenative coupling of 424
primary alcohols with secondary alcohols or amines, coupling of 425
diols and diamines, and coupling of amino alcohols with 426
secondary alcohols, according to Scheme 15.^{27,28,32–36,39} The 427 s15
dehydrogenative olefination of alcohols using a Wittig reagent 428
was demonstrated.⁴¹ Two miscellaneous catalytic reactions of 429
11 via 2 involved CO oxidation by N₂O and the selective 430
deuteration of alcohols in D₂O.^{31,43} Reactions of Scheme 15 431
were proposed to proceed via the initial formation of an 432
aromatized alkoxide complex from 2 and the substrate alcohol. 433
Although a major effort has been put into the study of the 434
catalytic activity of 2, little is known about the stoichiometric 435
reactivity of this complex. Addition of acetic or formic acid led to 436

Scheme 14. Hydrogenation Reactions with **2**^{3–5,26,29,30,38,40}Scheme 15. Dehydrogenative Coupling with **2** and **11**^{27,28,32–36,39,41}

dearomatization of the PNN ligand. Complexes **2** and **4** featured prominently in the catalytic cycles. Li and Hall⁴⁵ and Hasanayn with co-workers⁴⁸ investigated the catalytic oxidation of primary alcohols in aqueous NaOH, resulting in the corresponding carboxylates. Although the proposed mechanisms differed significantly, dihydride **4** was their common catalytic intermediate. Wang and co-workers⁴⁶ computed a mechanism of the pyrrole synthesis of Scheme 15. Once again, the ideas of MLC by aromatization–dearomatization were pursued. Alcohol dehydrogenation on **2** was proposed to follow the so-called BDFT (bifunctional double hydrogen transfer) mechanism to give **4**. Dub and Gordon²² re-examined the computation work of Wang and co-workers to point out that their “proton shuttle” was a nonexistent process. Finally, Gonçalves and Huang performed a computational analysis of the aromaticity changes upon the heterolytic H₂ cleavage on **2** to give **4**.⁴⁹ No study mentioned above was evidence-based.

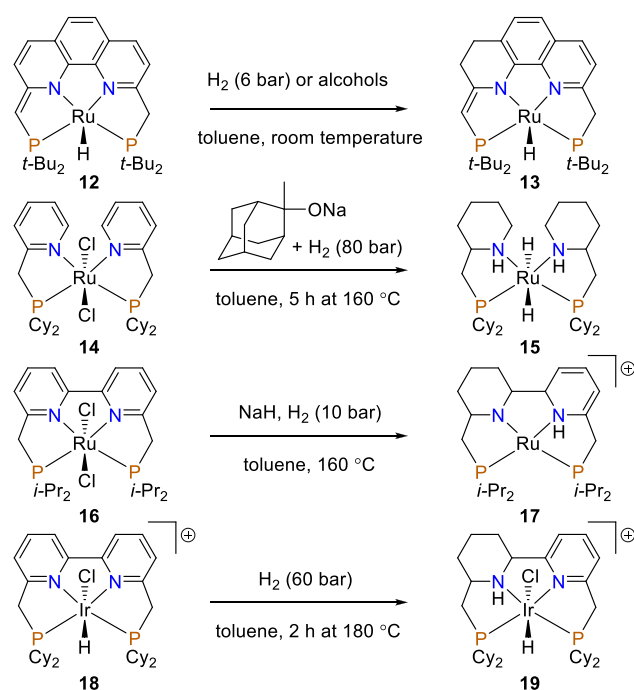
Our work does not imply that complex **2** itself is not a capable catalyst of ester hydrogenation and alcohol dehydrogenative coupling, without formation of a piperidine-type ligand. However, the sticking point of the calculated mechanisms is the assumption of sustained presence of catalytically relevant concentrations of **2** and **4** under H₂ or in alcohols over the 24–48 h reaction times of Schemes 14 and 15. The involvement of complexes **5**–**9** (and the intermediates leading to these complexes) in the catalytic reactions of Schemes 14 and 15 cannot be ignored. This situation serves as a warning that while DFT studies offer valuable insights, they can be biased, unduly narrow in scope, and inconclusive. This may happen when little is known about the underlying chemistry; however, the theoretical modeling can also be flawed. For example, a meaningful computational study of hydrogen ion (H⁺/H[−]) transfers and the resulting ionic reaction intermediates requires geometry optimizations in a solvent continuum, in conjunction with explicit solvation when hydrogen bonding is important. The relatively widespread gas-phase DFT modeling of MLC is inappropriate because the stationary points found in the gas phase may not exist in solution and vice versa.^{22,60–64,70}

The meaning of “cooperation” or “cooperativity” in MLC is somewhat open to interpretation, as the terms are not specific. The conventional MLC mechanisms²² with the Noyori-type systems seem to have one common feature: their catalytic cycles all include a formal 16-electron intermediate. Thus, “the *non-innocent* ligands directly participate in the substrate activation and in the bond formation.”⁶⁸ These ideas have been rebuked in recent years.^{22,60–64} The modern understanding of MLC is that the cooperating ligand is *innocent* in the catalytic hydrogenation and dehydrogenative coupling reactions with the Noyori-type catalysts. Our calculations are in full accord with this understanding. The five-coordinate amido complex **5a** is an off-cycle species in the mechanism of Scheme 9 where the catalyst is the dihydride complex **8**. Another important species in the cycle is alkoxide **9**·EtOH. We already extensively commented on this intermediate that should be thermodynamically and kinetically labile to allow facile regeneration of the dihydride catalyst under H₂.²⁵ All intermediates of Schemes 9 and 10 are octahedral Ru(II) complexes where the reacting organic moiety is hydrogen-bonded to the NH group of the pPN(H)N ligand which forms a reaction “pocket” where the substrate is optimally oriented, activated, or stabilized.

The hydrogenation of **2**, documented in this study, is not unprecedented. Similarly, the phenanthroline-based PNNP ligand of ruthenium complex **12** of Scheme 16 undergoes facile

the expected octahedral aromatized Ru(II) carboxylate complexes.^{35,36} Similarly, **2** with water gave the aromatized Ru(II) hydroxide.³⁶ Finally, addition of CO to **2** afforded the octahedral dearomatized dicarbonyl product.⁴³ No study of reactions of **2** with H₂ or alcohols has been disclosed.

Despite the scarcity of information about the reactivity of **2**, seven computational studies^{22,44–49} have been published to date that pursued different aspects of the catalytic mechanisms with **2**. Cantillo⁴⁴ and Zhang⁴⁷ independently modeled the catalytic hydrogenation of amides of Scheme 14. Both studies concluded that the reaction occurred via MLC involving aromatization/

Scheme 16. Examples of PNNP and PN Ligand Hydrogenation^{71–74}


511 hydrogenation under H₂ or when reacted with methanol or
 512 hexanol.⁷¹ The hydrogenation of **12** was not studied at 110 °C
 513 when this system becomes active for the dehydrogenative
 514 coupling of primary alcohols. Saito and co-workers observed
 515 hydrogenation of the pyridine and bipyridine fragments of
 516 ruthenium complexes **14** and **16** (Scheme 16) upon heating,
 517 under basic conditions, to give the Noyori-type catalysts **15** and
 518 **17**, respectively.^{72,73} The bipyridine fragment of **16** underwent a
 519 full hydrogenation and a P–C bond cleavage when the H₂
 520 pressure was increased to 40 bar.⁷³ The related iridium
 521 hydrido-chloride **18** was hydrogenated under base-free con-
 522 ditions, first to give **19** after 2 h, then a fully hydrogenated
 523 product after 4 h of heating.⁷⁴ Considering that the PNN ligand
 524 of **2** has been used to make manganese,^{75–78} iron,^{79–83} and
 525 cobalt^{84–88} catalysts, it is appropriate to suggest that mechanistic
 526 studies of these complexes must inquire into the nature of the
 527 metal species formed under conditions approximating the
 528 catalytic, i.e., using the relevant reaction temperature, time, and
 529 (when present) H₂ pressure.

530 In conclusion, our work and the examples of Scheme 16
 531 comprise substantive evidence indicating that the heteroar-
 532 omatic fragments of the coordinated PN, PNN, and related
 533 polydentate ligands may be susceptible to hydrogenation under
 534 reducing conditions. A notable exception is complex **3** that is
 535 relatively stable at 100 °C under 50 bar H₂. Theoretical studies
 536 of reactions of the metal complexes structurally related to **2**, **12**–
 537 **14**, and **16**–**19** should consider the previous studies detailing
 538 facile changes to the ligand architecture and should be supported
 539 by sufficient relevant experimental data.

540 ■ MATERIALS AND METHODS

541 **Experimental Details.** Complexes **2** and **3** were prepared following
 542 the reported procedures.^{3,25} All chemicals and solvents were purchased
 543 from Sigma-Aldrich. Anhydrous-grade solvents, ethyl acetate, and
 544 methyl hexanoate were stored and used in an argon drybox. The
 545 anhydrous deuterated solvents were stored and used in the same

drybox, with 3 Å molecular sieves. The room-temperature NMR spectra
 546 were collected on a Agilent DD2 400 MHz spectrometer, and the low-
 547 temperature studies were conducted on a Varian Unity Inova 300 MHz
 548 instrument. For quantitative integration, the proton NMR spectra were
 549 acquired using 15° pulses and a relaxation delay of 30 s. 550

Complex 5. In an argon glovebox, the glass liner of a 75 mL Parr
 551 reactor was loaded with a 9.5 mm × 13 mm SCIENCEWARE rare-earth
 552 magnet spinbar, 0.25 g (0.56 mmol) of **2**, and 4 mL of benzene. The
 553 reactor was closed, removed from the glovebox, pressurized to *p*(H₂) =
 554 50 bar, and placed in an oil bath preheated to 100 °C. After 2 h of
 555 stirring, the reactor was moved into a cold-water bath for 30 min, then
 556 vented and returned into the glovebox. The dark product solution and
 557 the spinbar were transferred into a 25 mL pear-shaped flask, and the
 558 solvent was evaporated under vacuum, followed by drying of the
 559 golden-yellow solid for 1 h. The product was redissolved in 12 mL of
 560 hexane, and the product solution was filtered through a medium-
 561 porosity fritted funnel into a 20 mL vial. This vial was left in the freezer
 562 (–25 °C) of the glovebox overnight. The product crystallized, and the
 563 mother liquor was removed from the vial with a pipet; the remaining
 564 yellow crystalline material was dried under vacuum for 2 h. Yield: 176
 565 mg (70%) of complex **5** containing ~8 mol % of residual hexane. 566
 Elemental analysis was not attempted on this material because of the
 567 residual solvent and extreme air-sensitivity. NMR data (main isomer
 568 **5a**): ¹H NMR (400 MHz; C₆D₆): δ 9.06 (m, 1H), 6.75 (td, *J* = 7.8, 1.6
 569 Hz, 1H), 6.59 (d, *J* = 7.8 Hz, 1H), 6.20 (t, *J* = 6.5 Hz, 1H), 3.90 (d, *J* =
 570 11.3 Hz, 1H), 3.30 (m, 1H), 2.25 (ddd, *J* = 14.6, 10.5, 5.4 Hz, 1H), 1.95
 571 (dm, *J* = 12.3, 1H), 1.84 (m, 2H), 1.67 (ddd, *J* = 14.6, 8.6, 7.6 Hz, 1H),
 572 1.52 (qt, *J* = 13.1, 3.7 Hz, 1H), 1.33 (d, *J* = 9.8 Hz, 9H), 1.30 (d, *J* = 9.9
 573 Hz, 9H), 1.14 (m, 1H), 1.00 (m, 1H), –18.48 (dt, *J* = 22.2, 2.2 Hz, 1H).
 574 ¹³C{¹H} NMR (100 MHz; C₆D₆): δ 209.5 (d, *J* = 11.5 Hz, CO), 171.7
 575 (d, *J* = 1.2 Hz, C), 154.0 (s, CH), 134.3 (s, CH), 121.6 (d, *J* = 2.1 Hz,
 576 CH), 120.9 (d, *J* = 1.0 Hz, CH), 74.6 (d, *J* = 3.3 Hz, NCH), 67.4 (d, *J* =
 577 6.3 Hz, NCH), 37.9 (d, *J* = 11.4 Hz, CH₂), 36.8 (d, *J* = 16.4 Hz, CH₂),
 578 35.9 (d, *J* = 18.7 Hz, C), 35.8 (d, *J* = 18.3 Hz, C), 33.7 (s, CH₂), 30.3
 579 (br, CH₃), 29.1 (d, *J* = 5.0 Hz, CH₃), 26.5 (d, *J* = 1.6 Hz, CH₂). ³¹P{¹H}
 580 NMR (162 MHz; C₆D₆): δ 118.1 (minor isomer), 113.2 (main
 581 isomer). 582

Complex 6. Crystalline **6** was obtained in two different ways. The
 583 first method closely followed the procedure reported above for **5** except
 584 that benzene was replaced by hexane. Crystals of **6** suitable for X-ray
 585 analysis formed in an NMR tube filled with the hexane product solution
 586 retrieved from the Parr reactor. The second sample of crystalline **6** was
 587 obtained from a benzene/hexane solvent mixture as follows. In an argon
 588 glovebox, anhydrous THF (10 mL) was pipetted into a 100 mL round-
 589 bottom flask containing **11** (0.6 g, 1.25 mmol) and *t*BuOK (0.18 g, 1.60
 590 mmol), and the mixture was magnetically stirred for 1 h. After solvent
 591 removal, the dark-green solid was dried for 1 h under vacuum. This
 592 material was extracted with 15 mL of benzene. The dark-green solution
 593 was filtered and transferred into the glass liner of a 300 mL Parr
 594 autoclave. Further 27 mL of hexane was added, and the reactor was
 595 removed from the glovebox, pressurized to 50 bar H₂, and left at room
 596 temperature for 4 h without heating or stirring. Next, the autoclave was
 597 depressurized, taken back into the glovebox, and opened to reveal
 598 a dark red-brown solution. The reactor was closed, repressurized to 50
 599 bar, and left at room temperature for 3 days. When the reactor was
 600 opened again in the argon glovebox, there was a dark brown solution
 601 and a cluster of large crystals at the bottom. The solution was decanted,
 602 and the crystals (~70 mg) were rinsed with hexane and collected into a
 603 vial. The product was characterized by X-ray diffraction and by NMR
 604 spectroscopy in C₆D₆ where the crystalline material is very sparingly
 605 soluble. The solubility was also poor in CD₂Cl₂ where the product
 606 decomposed. Although the principal resonances are well-defined in the
 607 ¹H NMR spectrum of **6**, there are areas of signal overlap where a
 608 detailed interpretation is challenging. The spectrum is also complicated
 609 by the resonances of the cocrystallized benzene and hexane. ¹H NMR
 610 (400 MHz; C₆D₆): δ 8.89 (d, *J* = 5.0 Hz, 1H), 6.99 (t, *J* = 7.8 Hz, 1H),
 611 6.93 (dd, *J* = 7.5, 1.1 Hz, 1H), 6.83 (m, 2H), 6.45 (m, 2H), 5.56 (t, *J* =
 612 5.2 Hz, 1H), 4.27 (dd, *J* = 16.9, 6.3 Hz, 1H), 3.77 (m, 2H), 3.68 (d, *J* =
 613 3.1 Hz, 1H), 3.57 (br, 1H), 3.26 (dd, *J* = 16.9, 11.0 Hz, 1H), 3.05 (q, *J* =
 614 11.8 Hz, 1H), 2.54 (m, 2H), 2.22 (m, 1H), 2.00 (m, 1H), 1.66 (m, 7H), 615

616 1.48 (m), 1.25 (dd, $J = 12.2$, 9H), 1.24 (dd, $J = 13.1$, 9H), 1.17 (d, $J =$
617 12.0, 9H), 1.15 (d, $J = 12.3$, 9H), -10.47 (ddd, $J = 23.4$, 19.0, 5.0 Hz,
618 1H), -12.20 (ddt, $J = 38.7$, 5.9, 5.2 Hz, 1H), -15.72 (dd, $J = 30.1$, 5.1
619 Hz, 1H). $^{31}\text{P}\{^1\text{H}\}$ NMR (162 MHz; C_6D_6): δ 113.6, 98.7.

620 **NMR Data for 7.** ^1H NMR (300 MHz; $\text{THF-}d_8$, -30 °C): δ 7.94 (d,
621 $J = 5.5$ Hz, 1H), 7.83 (d, $J = 6.0$ Hz, 1H), 7.06 (t, $J = 7.6$ Hz, 1H), 6.94
622 (t, $J = 7.6$ Hz, 1H), 6.80 (d, $J = 8.2$ Hz, 1H), 6.74 (d, $J = 8.2$ Hz, 1H),
623 6.68 (m, 2H), 6.65 (d, $J = 6.7$ Hz, 1H), 6.58 (d, $J = 8.5$ Hz, 1H), 6.47 (d,
624 $J = 7.1$ Hz, 1H), 6.40 (t, $J = 6.3$ Hz, 1H), 6.01 (m, 2H), 3.21 (dd, $J =$
625 11.4, 15.5 Hz, 1H), 3.07 (dd, $J = 11.4$, 15.6 Hz, 1H), 2.49 (dd, $J = 7.9$,
626 15.5 Hz, 1H), 2.37 (dd, $J = 6.7$, 15.6 Hz, 1H), 1.60 (d, $J = 12.0$ Hz,
627 CH_3), 1.25 (br, CH_3), 1.07 (br, CH_3), 0.86 (d, $J = 11.5$ Hz, CH_3),
628 -13.40 (ddd, $J = 2.4$, 16.0, 23.7 Hz, 1H), -20.05 (ddd, $J = 4.3$, 12.1,
629 16.0 Hz, 1H). $^{31}\text{P}\{^1\text{H}\}$ NMR (300 MHz; $\text{THF-}d_8$): δ 104.8 (s), 122.7
630 (s).

631 **NMR Data for 9 (Main Species) Formed upon Dissolving 5 in**
632 **Ethanol- d_6 .** ^1H NMR (400 MHz; ethanol- d_6): δ 9.01 (m, 1H, Py),
633 7.84 (td, $J = 7.8$, 1.6 Hz, 1H, Py), 7.34 (overlapped m, 2H, Py), 3.98 (d, J
634 $= 11.6$ Hz, 1H, NCH), 3.06 (t, $J = 11.6$ Hz, 1H, NCH), 2.40–1.63 (m,
635 8H, CH_2), 1.38 (d, $J = 13.2$ Hz, 9H, CH_3), 1.35 (d, $J = 13.2$ Hz, 9H,
636 CH_3), -16.68 (d, $J = 26$ Hz, 1H). $^{13}\text{C}\{^1\text{H}\}$ NMR (100 MHz; ethanol-
637 d_6): δ 206.5 (d, $J = 15.7$ Hz, CO), 164.6, 153.5, 137.7, 124.0, 121.8 (Py),
638 69.0 (d, $J = 2.9$ Hz, NCH), 65.1 (m, NCH), 38.0 (d, $J = 14.7$ Hz, C, t -
639 Bu), 37.6 (d, $J = 23.9$ Hz, C, t -Bu), 34.4 (d, $J = 15.1$ Hz, CH_2), 32.3 (d, J
640 $= 11.9$ Hz, CH_2), 30.4 (d, $J = 4.6$ Hz, CH_3 , t -Bu), 30.3 (d, $J = 3.4$ Hz,
641 CH_3 , t -Bu), 28.2 (s, CH_2), 25.4 (s, CH_2). Resonances of the
642 Ru(OC_2D_5) group were not observed due to exchange with the
643 solvent. $^{31}\text{P}\{^1\text{H}\}$ NMR (162 MHz; ethanol- d_6): δ 98.5 (s).

644 **NMR Data for 10 Formed on Heating 2 in EtOH for 6 h at 80**
645 **°C.** ^1H NMR (400 MHz; EtOH): δ 9.00 (m, 1H, Py), 7.84 (td, $J = 7.8$,
646 1.6 Hz, 1H, Py), 7.34 (overlapped m, 2H, Py), 3.99 (d, $^3J = 11.2$ Hz, 1H,
647 NCH), 3.05 (t, $^3J = 12.2$ Hz, 1H, NCH), 2.44–1.63 (m, 8H, CH_2), 1.35
648 (d, $^3J = 12.8$ Hz, 9H, CH_3), 1.31 (d, $^3J = 13.0$ Hz, 9H, CH_3), -17.56 (d,
649 $^2J = 26.4$ Hz, 1H). $^{13}\text{C}\{^1\text{H}\}$ NMR (100 MHz; EtOH): δ 205 (d, $^2J =$
650 14.9 Hz, CO), 181.9 (s, OAc), 164.4, 153.7, 137.5, 124.0, 120.9 (Py),
651 68.1 (d, $J = 3.1$ Hz, NCH), 64.1 (d, $J = 2.6$ Hz, NCH), 37.2 (d, $J = 23.7$
652 Hz, C, t -Bu), 37.0 (d, $J = 15.3$ Hz, C, t -Bu), 34.3 (d, $J = 15.7$ Hz, CH_2),
653 32.3 (d, $J = 12.1$ Hz, CH_2), 29.7 (d, $J = 3.3$ Hz, CH_3 , t -Bu), 29.4 (d, $J =$
654 4.5 Hz, CH_3 , t -Bu), 28.4 (s, CH_2), 24.9 (s, CH_2), 25.4 (s, OAc).
655 $^{31}\text{P}\{^1\text{H}\}$ NMR (162 MHz; ethanol- d_6): δ 100.1 (s)

656 **Hydrogenation.** The hydrogenations of ethyl acetate and methyl
657 hexanoate were performed in a 300 mL stainless-steel Parr reactor.
658 Inside an argon glovebox, the required quantities of the catalysts (9–10
659 mg) were weighed out on a calibrated analytical balance accurate to 0.1
660 mg. A balance accurate to 1 mg was used for taking 0.2 mol of the esters
661 (prior to weighing, the ester substrate was allowed to pass through a
662 layer of activated basic alumina). The reactor was loaded with a 0.95 cm
663 \times 2.54 cm SCIENCEWARE rare-earth magnet spinbar, the catalyst,
664 and the ester substrate; it was assembled inside the glovebox, then taken
665 outside and pressurized under H_2 to 50 bar. The pressurized reactor was
666 disconnected from the H_2 tank and placed into an oil bath preheated to
667 100 °C on a hot plate stirrer. This temperature was maintained for 3 h
668 while magnetically stirring at 500 rpm.

669 **Computational Details.** All calculated ruthenium species of this
670 paper possess a zero net charge. The DFT calculations were carried out
671 with Gaussian 16, revision c.01,⁸⁹ using the M06-L^{67,90} and M06-2X
672 functionals.⁶⁶ The basis sets used for the initial geometry optimization
673 and frequency calculations on the ruthenium species included def2-
674 QZVP (with def2 ECP) for Ru, and def2-TZVP for all other atoms
675 (together with the W06 density fitting basis set).^{91,92} Subsequently, all
676 geometries were reoptimized using the def2-QZVP basis set for all
677 atoms. The polarizable continuum model (asymmetric isotropic
678 IEFPCM) was used in all (except H_2) geometry optimizations and
679 frequency calculations, with the radii and nonelectrostatic terms of
680 Truhlar and co-workers' SMD solvation model (scrf = smd).⁹³ An
681 example of a typical g16 input file is provided in the [Supporting](#)
682 [Information](#). The reported energies of the ruthenium species were
683 obtained by combining the electronic energies of the structures
684 optimized at the M06-L/def2-QZVP level with the thermal corrections
685 from the frequency calculations, plus the standard state correction^{94,95}

of 1.89 kcal/mol. The standard state correction for ethyl acetate was 686
3.27 kcal/mol when the ester was both the substrate and the solvent, in 687
[Schemes 9–13](#). All organic molecules (acetaldehyde, ethanol, ethyl 688
acetate, 1-ethoxyethanol) and TS9 were optimized using the M06-L/ 689
def2-QZVP and M06-2X/def2-QZVP methods, followed by frequency 690
calculations at the same level of theory. The nature of the following 691
transition states TS2, TS4, TS5, and TS11 was confirmed by intrinsic 692
reaction coordinate (IRC) calculations. Dynamics has not been taken 693
into account when modeling the structures with the explicit, hydrogen- 694
bonded ethanol. 695

■ ASSOCIATED CONTENT

Supporting Information

The Supporting Information is available free of charge at 698
<https://pubs.acs.org/doi/10.1021/jacs.0c06518>. 699

Representative NMR spectra, computed energies, and a 700
summary of the crystal data collection and refinement 701
parameters for 5, 6, and 7 (PDF) 702

Crystallographic data for 5, 6, and 7 (CIF) 703

File structures.xyz containing Cartesian coordinates of the 704
metal complexes computed in this study, where this file 705
may be opened as a text file to read the coordinates or 706
opened directly by a molecular modeling program such as 707
Mercury (<http://www.ccdc.cam.ac.uk/pages/Home.aspx>) for visualization and analysis (XYZ) 708
709

■ AUTHOR INFORMATION

Corresponding Authors

Eugene Khaskin – Okinawa Institute of Science and Technology, 712
Okinawa 904-0495, Japan; orcid.org/0000-0003-1790-704X; Email: eugene.khaskin@oist.jp 713
714

Dmitry G. Gusev – Department of Chemistry and Biochemistry, 715
Wilfrid Laurier University, Waterloo, ON N2L 3C5, Canada; 716
orcid.org/0000-0003-3302-356X; Email: dgoussev@wlu.ca 717
718

Authors

Louise N. Dawe – Department of Chemistry and Biochemistry, 720
Wilfrid Laurier University, Waterloo, ON N2L 3C5, Canada; 721
orcid.org/0000-0003-3630-990X 722

Morteza Karimzadeh-Younjali – Department of Chemistry and 723
Biochemistry, Wilfrid Laurier University, Waterloo, ON N2L 724
3C5, Canada 725

Zengjin Dai – Department of Chemistry and Biochemistry, 726
Wilfrid Laurier University, Waterloo, ON N2L 3C5, Canada 727

Complete contact information is available at: 728

<https://pubs.acs.org/doi/10.1021/jacs.0c06518> 729

Funding

Natural Sciences and Engineering Research Council (NSERC) 731
of Canada, Discovery grant program, and Compute Canada. 732

Notes

The authors declare no competing financial interest. 733
734

■ ACKNOWLEDGMENTS

D.G.G. is thankful to the NSERC of Canada—Discovery grant 736
program, CFI LOF program, Compute Canada, and Wilfrid 737
Laurier University for support. Dr. Paul D. Boyle, the University 738
of Western Ontario, is acknowledged for assistance with the X- 739
ray data collection. 740

741 ■ REFERENCES

- 742 (1) Zhang, J.; Leitus, G.; Ben-David, Y.; Milstein, D. Facile
743 Conversion of Alcohols into Esters and Dihydrogen Catalyzed by
744 New Ruthenium Complexes. *J. Am. Chem. Soc.* **2005**, *127*, 10840–
745 10841.
- 746 (2) Zhang, J.; Leitus, G.; Ben-David, Y.; Milstein, D. Efficient
747 Homogeneous Catalytic Hydrogenation of Esters to Alcohols. *Angew.*
748 *Chem., Int. Ed.* **2006**, *45*, 1113–1115.
- 749 (3) Balaraman, E.; Gnanaprakasam, B.; Shimon, L. J. W.; Milstein, D.
750 Direct Hydrogenation of Amides to Alcohols and Amines under Mild
751 Conditions. *J. Am. Chem. Soc.* **2010**, *132*, 16756–16758.
- 752 (4) Balaraman, E.; Ben-David, Y.; Milstein, D. Unprecedented
753 Catalytic Hydrogenation of Urea Derivatives to Amines and Methanol.
754 *Angew. Chem., Int. Ed.* **2011**, *50*, 11702–11705.
- 755 (5) Balaraman, E.; Gunanathan, C.; Zhang, J.; Shimon, L. J. W.;
756 Milstein, D. Efficient Hydrogenation of Organic Carbonates,
757 Carbamates and Formates Indicates Alternative Routes to Methanol
758 Based on CO₂ and CO. *Nat. Chem.* **2011**, *3*, 609–614.
- 759 (6) Milstein, D. Discovery of Environmentally Benign Catalytic
760 Reactions of Alcohols Catalyzed by Pyridine-Based Pincer Ru
761 Complexes, Based on Metal–Ligand Cooperation. *Top. Catal.* **2010**,
762 *53*, 915–923.
- 763 (7) Gunanathan, C.; Milstein, D. Bond Activation by Metal–Ligand
764 Cooperation: Design of “Green” Catalytic Reactions Based on
765 Aromatization–Dearomatization of Pincer Complexes. *Top. Organo-*
766 *met. Chem.* **2011**, *37*, 55–84.
- 767 (8) Gunanathan, C.; Milstein, D. Metal–Ligand Cooperation by
768 Aromatization–Dearomatization: A New Paradigm in Bond Activation
769 and “Green” Catalysis. *Acc. Chem. Res.* **2011**, *44*, 588–602.
- 770 (9) Gunanathan, C.; Milstein, D. Bond Activation and Catalysis by
771 Ruthenium Pincer Complexes. *Chem. Rev.* **2014**, *114*, 12024–12087.
- 772 (10) Gunanathan, C.; Milstein, D. Catalysis by Pincer Complexes:
773 Synthesis of Esters, Amides, and Peptides. In *Pincer and Pincer-Type*
774 *Complexes: Applications in Organic Synthesis and Catalysis*; Szabó, K. J.,
775 Wendt, O. F., Eds.; Wiley-VCH Verlag GmbH & Co. KGaA, 2014.
- 776 (11) Khusnutdinova, J. R.; Milstein, D. Metal–Ligand Cooperation.
777 *Angew. Chem., Int. Ed.* **2015**, *54*, 12236–12273.
- 778 (12) Milstein, D. Metal–Ligand Cooperation by Aromatization–
779 Dearomatization as a Tool in Single Bond Activation. *Philos. Trans. R.*
780 *Soc., A* **2015**, *373*, 20140189.
- 781 (13) Grützmacher, H. Cooperating Ligands in Catalysis. *Angew.*
782 *Chem., Int. Ed.* **2008**, *47*, 1814–1818.
- 783 (14) Gelman, D.; Musa, S. Coordination Versatility of sp³-Hybridized
784 Pincer Ligands toward Ligand–Metal Cooperative Catalysis. *ACS*
785 *Catal.* **2012**, *2*, 2456–2466.
- 786 (15) Dub, P. A.; Ikariya, T. Catalytic Reductive Transformations of
787 Carboxylic and Carbonic Acid Derivatives Using Molecular Hydrogen.
788 *ACS Catal.* **2012**, *2*, 1718–1741.
- 789 (16) Eisenstein, O.; Crabtree, R. H. Outer Sphere Hydrogenation
790 Catalysis. *New J. Chem.* **2013**, *37*, 21–27.
- 791 (17) Werkmeister, S.; Junge, K.; Beller, M. Catalytic Hydrogenation of
792 Carboxylic Acid Esters, Amides, and Nitriles with Homogeneous
793 Catalysts. *Org. Process Res. Dev.* **2014**, *18*, 289–302.
- 794 (18) Trincado, M.; Banerjee, D.; Grützmacher, H. Molecular
795 Catalysts for Hydrogen Production from Alcohols. *Energy Environ.*
796 *Sci.* **2014**, *7*, 2464–2503.
- 797 (19) Werkmeister, S.; Neumann, J.; Junge, K.; Beller, M. Pincer-Type
798 Complexes for Catalytic (De)Hydrogenation and Transfer (De)-
799 Hydrogenation Reactions: Recent Progress. *Chem. - Eur. J.* **2015**, *21*,
800 12226–12250.
- 801 (20) Younus, H. A.; Su, W.; Ahmad, N.; Chen, S.; Verpoort, F.
802 Ruthenium Pincer Complexes: Synthesis and Catalytic Applications.
803 *Adv. Synth. Catal.* **2015**, *357*, 283–330.
- 804 (21) Crabtree, R. H. Homogeneous Transition Metal Catalysis of
805 Acceptorless Dehydrogenative Alcohol Oxidation: Applications in
806 Hydrogen Storage and to Heterocycle Synthesis. *Chem. Rev.* **2017**, *117*,
807 9228–9246.
- 808 (22) Dub, P. A.; Gordon, J. C. Metal–Ligand Bifunctional Catalysis:
809 The “Accepted” Mechanism, the Issue of Concertedness, and the
Function of the Ligand in Catalytic Cycles Involving Hydrogen Atoms. *ACS*
Catal. **2017**, *7*, 6635–6655. 810
- (23) Hale, L. V. A.; Szymczak, N. K. Hydrogen Transfer Catalysis
811 beyond the Primary Coordination Sphere. *ACS Catal.* **2018**, *8*, 6446–
812 6461. 813
- (24) Li, J.; Shiota, Y.; Yoshizawa, K. Metal–Ligand Cooperation in H₂
814 Production and H₂O Decomposition on a Ru(II) PNN Complex: The
815 Role of Ligand Dearomatization–Aromatization. *J. Am. Chem. Soc.* **2009**,
816 *131*, 13584–13585. 817
- (25) Gusev, D. G. Revised Mechanisms of the Catalytic Alcohol
818 Dehydrogenation and Ester Reduction with the Milstein PNN
819 Complex of Ruthenium. *Organometallics* **2020**, *39*, 258–270. 820
- (26) Huff, C. A.; Sanford, M. S. Cascade Catalysis for the
821 Homogeneous Hydrogenation of CO₂ to Methanol. *J. Am. Chem. Soc.* **2011**,
822 *133*, 18122–18125. 823
- (27) Gnanaprakasam, B.; Balaraman, E.; Gunanathan, C.; Milstein, D.
824 Synthesis of Polyamides from Diols and Diamines with Liberation of
825 H₂. *J. Polym. Sci., Part A: Polym. Chem.* **2012**, *50*, 1755–1765. 826
- (28) Srimani, D.; Balaraman, E.; Gnanaprakasam, B.; Ben-David, Y.;
827 Milstein, D. Ruthenium Pincer-Catalyzed Cross-Dehydrogenative
828 Coupling of Primary Alcohols with Secondary Alcohols under Neutral
829 Conditions. *Adv. Synth. Catal.* **2012**, *354*, 2403–2406. 830
- (29) Balaraman, E.; Fogler, E.; Milstein, D. Efficient Hydrogenation of
831 Biomass-Derived Cyclic Di-Esters to 1,2-Diols. *Chem. Commun.* **2012**,
832 *48*, 1111–1113. 833
- (30) Srimani, D.; Feller, M.; Ben-David, Y.; Milstein, D. Catalytic
834 Coupling of Nitriles with Amines to Selectively Form Imines Under
835 Mild Hydrogen Pressure. *Chem. Commun.* **2012**, *48*, 11853–11855. 836
- (31) Khaskin, E.; Milstein, D. Simple and Efficient Catalytic Reaction
837 for the Selective Deuteration of Alcohols. *ACS Catal.* **2013**, *3*, 448–452. 838
- (32) Srimani, D.; Balaraman, E.; Hu, P.; Ben-David, Y.; Milstein, D.
839 Formation of Tertiary Amides and Dihydrogen by Dehydrogenative
840 Coupling of Primary Alcohols with Secondary Amines Catalyzed by
841 Ruthenium Bipyridine-Based Pincer Complexes. *Adv. Synth. Catal.* **2013**,
842 *355*, 2525–2530. 843
- (33) Srimani, D.; Ben-David, Y.; Milstein, D. Direct Synthesis of
844 Pyrroles by Dehydrogenative Coupling of β-Aminoalcohols with
845 Secondary Alcohols Catalyzed by Ruthenium Pincer Complexes. *Angew.*
846 *Chem., Int. Ed.* **2013**, *52*, 4012–4015. 847
- (34) Srimani, D.; Ben-David, Y.; Milstein, D. Direct Synthesis of
848 Pyridines and Quinolines by Coupling of γ-Amino-alcohols with
849 Secondary Alcohols Liberating H₂ Catalyzed by Ruthenium Pincer
850 Complexes. *Chem. Commun.* **2013**, *49*, 6632–6634. 851
- (35) Balaraman, E.; Khaskin, E.; Leitus, G.; Milstein, D. Catalytic
852 Transformation of Alcohols to Carboxylic Acid Salts and H₂ Using
853 Water as the Oxygen Atom Source. *Nat. Chem.* **2013**, *5*, 122–125. 854
- (36) Hu, P.; Diskin-Posner, Y.; Ben-David, Y.; Milstein, D. Reusable
855 Homogeneous Catalytic System for Hydrogen Production from
856 Methanol and Water. *ACS Catal.* **2014**, *4*, 2649–2652. 857
- (37) Srimani, D.; Leitus, G.; Ben-David, Y.; Milstein, D. Direct
858 Catalytic Olefination of Alcohols with Sulfones. *Angew. Chem., Int. Ed.* **2014**,
859 *53*, 11092–11095. 860
- (38) Krall, E. M.; Klein, T. W.; Andersen, R. J.; Nett, A. J.; Glasgow, R.
861 W.; Reader, D. S.; Dauphinais, B. C.; Mc Ilrath, S. P.; Fischer, A. A.;
862 Carney, M. J.; Hudson, D. J.; Robertson, N. J. Controlled Hydro-
863 genative Depolymerization of Polyesters and Polycarbonates Catalyzed
864 by Ruthenium(II) PNN Pincer Complexes. *Chem. Commun.* **2014**, *50*,
865 4884–4887. 866
- (39) Balaraman, E.; Srimani, D.; Diskin-Posner, Y.; Milstein, D. Direct
867 Synthesis of Secondary Amines From Alcohols and Ammonia
868 Catalyzed by a Ruthenium Pincer Complex. *Catal. Lett.* **2015**, *145*,
869 139–144. 870
- (40) Khusnutdinova, J. R.; Garg, J. A.; Milstein, D. Combining Low-
871 Pressure CO₂ Capture and Hydrogenation to Form Methanol. *ACS*
872 *Catal.* **2015**, *5*, 2416–2422. 873
- (41) Khaskin, E.; Milstein, D. Catalytic, Oxidant-Free, Direct
874 Olefination of Alcohols using Wittig Reagents. *Chem. Commun.* **2015**,
875 *51*, 9002–9005. 876

- 878 (42) Hu, P.; Ben-David, Y.; Milstein, D. Rechargeable Hydrogen
879 Storage System Based on the Dehydrogenative Coupling of Ethyl-
880 enediamine with Ethanol. *Angew. Chem., Int. Ed.* **2016**, *55*, 1061–1064.
- 881 (43) Zeng, R.; Feller, M.; Diskin-Posner, Y.; Shimon, L. J. W.; Ben-
882 David, Y.; Milstein, D. CO Oxidation by N₂O Homogeneously
883 Catalyzed by Ruthenium Hydride Pincer Complexes Indicating a New
884 Mechanism. *J. Am. Chem. Soc.* **2018**, *140*, 7061–7064.
- 885 (44) Cantillo, D. Mechanistic Insights on the Ruthenium-Catalyzed
886 Hydrogenation of Amides – C–N vs. C–O Cleavage. *Eur. J. Inorg.*
887 *Chem.* **2011**, *2011*, 3008–3013.
- 888 (45) Li, H.; Hall, M. B. Mechanism of the Formation of Carboxylate
889 from Alcohols and Water Catalyzed by a Bipyridine-Based Ruthenium
890 Complex: A Computational Study. *J. Am. Chem. Soc.* **2014**, *136*, 383–
891 395.
- 892 (46) Qu, S.; Dang, Y.; Song, C.; Wen, M.; Huang, K.-W.; Wang, Z.-X.
893 Catalytic Mechanisms of Direct Pyrrole Synthesis via Dehydrogenative
894 Coupling Mediated by PNP-Ir or PNN-Ru Pincer Complexes: Crucial
895 Role of Proton-Transfer Shuttles in the PNP-Ir System. *J. Am. Chem.*
896 *Soc.* **2014**, *136*, 4974–4991.
- 897 (47) Zhang, H. A. DFT study on direct hydrogenation of amide
898 catalyzed by a PNN Ru(II) pincer complex. *Comput. Theor. Chem.*
899 **2015**, *1066*, 1–6.
- 900 (48) Hasanayn, F.; Al-Assi, L. M.; Moussawi, R. N.; Omar, B. S.
901 Mechanism of Alcohol–Water Dehydrogenative Coupling into
902 Carboxylic Acid Using Milstein's Catalyst: A Detailed Investigation
903 of the Outer-Sphere PES in the Reaction of Aldehydes with an
904 Octahedral Ruthenium Hydroxide. *Inorg. Chem.* **2016**, *55*, 7886–7902.
- 905 (49) Gonçalves, T. P.; Huang, K.-W. Metal–Ligand Cooperative
906 Reactivity in the (Pseudo)-Dearomatized PNx(P) Systems: The
907 Influence of the Zwitterionic Form in Dearomatized Pincer Complexes.
908 *J. Am. Chem. Soc.* **2017**, *139*, 13442–13449.
- 909 (50) Spasyuk, D.; Smith, S.; Gusev, D. G. From Esters to Alcohols and
910 Back with Ruthenium and Osmium Catalysts. *Angew. Chem., Int. Ed.*
911 **2012**, *51*, 2772–2775.
- 912 (51) Spasyuk, D.; Gusev, D. G. Acceptorless Dehydrogenative
913 Coupling of Ethanol and Hydrogenation of Esters and Imines.
914 *Organometallics* **2012**, *31*, 5239–5242.
- 915 (52) Spasyuk, D.; Vicent, C.; Gusev, D. G. Chemoselective
916 Hydrogenation of Carbonyl Compounds and Acceptorless Dehydro-
917 genative Coupling of Alcohols. *J. Am. Chem. Soc.* **2015**, *137*, 3743–
918 3746.
- 919 (53) Gusev, D. G. Dehydrogenative Coupling of Ethanol and Ester
920 Hydrogenation Catalyzed by Pincer-type YNP Complexes. *ACS Catal.*
921 **2016**, *6*, 6967–6981.
- 922 (54) Wang, Z.; Li, Y.; Liu, Q.; Solan, G. A.; Ma, Y.; Sun, W. Direct
923 Hydrogenation of a Broad Range of Amides under Base-free
924 Conditions using an Efficient and Selective Ruthenium(II) Pincer
925 Catalyst. *ChemCatChem* **2017**, *9*, 4275–4281.
- 926 (55) Wang, Z.; Chen, X.; Liu, B.; Liu, Q.; Solan, G. A.; Yang, X.; Sun,
927 W. Cooperative Interplay Between a Flexible PNN-Ru(II) Complex
928 and a NaBH₄ Additive in the Efficient Catalytic Hydrogenation of
929 Esters. *Catal. Sci. Technol.* **2017**, *7*, 1297–1304.
- 930 (56) He, T.; Buttner, J. C.; Reynolds, E. F.; Pham, J.; Malek, J. C.;
931 Keith, J. M.; Chianese, A. R. Dehydroalkylative Activation of CNN- and
932 PNN-Pincer Ruthenium Catalysts for Ester Hydrogenation. *J. Am.*
933 *Chem. Soc.* **2019**, *141*, 17404–17413.
- 934 (57) Nguyen, D. H.; Trivelli, X.; Capet, F.; Swesi, Y.; Favre-Réguillon,
935 A.; Vanoye, L.; Dumeignil, F.; Gauvin, R. M. Deeper Mechanistic
936 Insight into Ru Pincer-Mediated Acceptorless Dehydrogenative
937 Coupling of Alcohols: Exchanges, Intermediates, and Deactivation
938 Species. *ACS Catal.* **2018**, *8*, 4719–4734.
- 939 (58) Zweifel, T.; Naubron, J.-V.; Büttner, T.; Ott, T.; Grützmacher, H.
940 Ethanol as Hydrogen Donor: Highly Efficient Transfer Hydrogenations
941 with Rhodium(I) Amides. *Angew. Chem., Int. Ed.* **2008**, *47*, 3245–3249.
- 942 (59) Hasanayn, F.; Baroudi, A. Direct H/OR and OR/OR' Metathesis
943 Pathways in Ester Hydrogenation and Transesterification by Milstein's
944 Catalyst. *Organometallics* **2013**, *32*, 2493–2496.
- 945 (60) Dub, P. A.; Henson, N. J.; Martin, R. L.; Gordon, J. C.
946 Unravelling the Mechanism of the Asymmetric Hydrogenation of
Acetophenone by [RuX₂(diphosphine)(1,2-diamine)] Catalysts. *J. Am.*
Chem. Soc. **2014**, *136*, 3505–3521.
- (61) Dub, P. A.; Gordon, J. C. The Mechanism of Enantioselective
Ketone Reduction with Noyori and Noyori-Ikariya Bifunctional
Catalysts. *Dalton Trans.* **2016**, *45*, 6756–6781.
- (62) Dub, P. A.; Scott, B. L.; Gordon, J. C. Why Does Alkylation of the
N-H Functionality within M/NH Bifunctional Noyori-Type Catalysts
Lead to Turnover? *J. Am. Chem. Soc.* **2017**, *139*, 1245–1260.
- (63) Dub, P. A.; Gordon, J. C. The Role of the Metal-Bound N–H
Functionality in Noyori-type Molecular Catalysts. *Nat. Rev. Chem.*
2018, *2*, 396–408.
- (64) Dub, P. A.; Batrice, R. J.; Gordon, J. C.; Scott, B. L.; Minko, Y.;
Schmidt, J. G.; Williams, R. F. Engineering Catalysts for Selective Ester
Hydrogenation. *Org. Process Res. Dev.* **2020**, *24* (3), 415–442.
- (65) Morris, S. A.; Gusev, D. G. Rethinking the Claisen–Tishchenko
Reaction. *Angew. Chem., Int. Ed.* **2017**, *56*, 6228–6231.
- (66) Zhao, Y.; Truhlar, D. G. The M06 Suite of Density Functionals
for Main Group Thermochemistry, Thermochemical Kinetics, Non-
covalent Interactions, Excited States, and Transition Elements: Two
New Functionals and Systematic Testing of Four M06-class Func-
tionals and 12 Other Functionals. *Theor. Chem. Acc.* **2008**, *120*, 215–
241.
- (67) Gusev, D. G. Assessing the Accuracy of M06-L Thermochem-
istry. *Organometallics* **2013**, *32*, 4239–4243.
- (68) Ikariya, T. Bifunctional Transition Metal-Based Molecular
Catalysts for Asymmetric Syntheses. *Top. Organomet. Chem.* **2011**,
37, 31–53.
- (69) *Hydrogen and Deuterium*; Young, C. L., Ed.; IUPAC Solubility
Data Series, Vol. 5/6; Pergamon Press: New York, 1981; p 231.
- (70) Ribeiro, R. F.; Marenich, A. V.; Cramer, C. J.; Truhlar, D. G. Use
of Solution-Phase Vibrational Frequencies in Continuum Models for
the Free Energy of Solvation. *J. Phys. Chem. B* **2011**, *115*, 14556–14562.
- (71) Langer, R.; Fuchs, I.; Vogt, M.; Balaraman, E.; Diskin-Posner, Y.;
Shimon, L. J. W.; Ben-David, Y.; Milstein, D. Stepwise Metal–Ligand
Cooperation by a Reversible Aromatization/Deconjugation Sequence
in Ruthenium Complexes with a Tetradentate Phenanthroline-Based
Ligand. *Chem. - Eur. J.* **2013**, *19*, 3407–3414.
- (72) Miura, T.; Held, I. E.; Oishi, S.; Naruto, M.; Saito, S. Catalytic
Hydrogenation of Unactivated Amides Enabled by Hydrogenation of
Catalyst Precursor. *Tetrahedron Lett.* **2013**, *54*, 2674–2678.
- (73) Miura, T.; Naruto, M.; Toda, K.; Shimomura, T.; Saito, S.
Multifaceted Catalytic Hydrogenation of Amides via Diverse Activation
of a Sterically Confined Bipyridine–Ruthenium Framework. *Sci. Rep.*
2017, *7*, 1586.
- (74) Nimura, S.; Yoshioka, S.; Naruto, M.; Saito, S. Reaction of H₂
with Mitochondria-Relevant Metabolites using a Multifunctional
Molecular Catalyst. *ChemRxiv* **2020**, DOI: 10.26434/chem-
rxiv.11994471.v1.
- (75) Das, U. K.; Ben-David, Y.; Diskin-Posner, Y.; Milstein, D. N-
substituted Hydrazones by Manganese-Catalyzed Coupling of
Alcohols with Hydrazine: Borrowing Hydrogen and Acceptorless
Dehydrogenation in One System. *Angew. Chem., Int. Ed.* **2018**, *57*,
2179–2182.
- (76) Das, U. K.; Ben-David, Y.; Leitus, G.; Diskin-Posner, Y.; Milstein,
D. Dehydrogenative Cross-Coupling of Primary Alcohols To Form
Cross-Esters Catalyzed by a Manganese Pincer Complex. *ACS Catal.*
2019, *9*, 479–484.
- (77) Das, U. K.; Kumar, A.; Ben-David, Y.; Iron, M. A.; Milstein, D.
Manganese Catalyzed Hydrogenation of Carbamates and Urea
Derivatives. *J. Am. Chem. Soc.* **2019**, *141*, 12962–12966.
- (78) Das, U. K.; Janes, T.; Kumar, A.; Milstein, D. Manganese
Catalyzed Selective Hydrogenation of Cyclic Imides to Diols and
Amines. *Green Chem.* **2020**, *22*, 3079–3082.
- (79) Zhang, L.; Peng, D.; Leng, X.; Huang, Z. Iron-Catalyzed, Atom-
Economical, Chemo- and Regioselective Alkene Hydroboration with
Pinacolborane. *Angew. Chem., Int. Ed.* **2013**, *52*, 3676–3680.
- (80) Zell, T.; Langer, R.; Iron, M. A.; Konstantinovskii, L.; Shimon, L.
J. W.; Diskin-Posner, Y.; Leitus, G.; Balaraman, E.; Ben-David, Y.;
Milstein, D. Synthesis, Structures, and Dearomatization by Deproto-

- 1016 nation of Iron Complexes Featuring Bipyridine-based PNN Pincer
1017 Ligands. *Inorg. Chem.* **2013**, *52*, 9636–9649.
- 1018 (81) Jia, X.; Zhang, L.; Qin, C.; Leng, X.; Huang, Z. Iridium
1019 Complexes of New NCP Pincer Ligands: Catalytic Alkane Dehydro-
1020 genation and Alkene Isomerization. *Chem. Commun.* **2014**, *50*, 11056–
1021 11059.
- 1022 (82) Zell, T.; Milko, P.; Fillman, K. L.; Diskin-Posner, Y.; Bendikov,
1023 T.; Iron, M. A.; Leitun, G.; Ben-David, Y.; Neidig, M. L.; Milstein, D.
1024 Iron Dicarbonyl Complexes Featuring Bipyridine-Based PNN Pincer
1025 Ligands with Short Interpyridine CC Bond Lengths: Innocent or Non-
1026 Innocent Ligand? *Chem. - Eur. J.* **2014**, *20*, 4403–4413.
- 1027 (83) Cummins, A. W. M.; Li, S.; Willcox, D. R.; Muilu, T.; Docherty, J.
1028 H.; Thomas, S. P. Synthesis of DBpin Using Earth-abundant Metal
1029 Catalysis. *Tetrahedron* **2020**, *76*, 131084.
- 1030 (84) Zhang, L.; Zuo, Z.; Leng, X.; Huang, Z. A Cobalt-Catalyzed
1031 Alkene Hydroboration with Pinacolborane. *Angew. Chem., Int. Ed.*
1032 **2014**, *53*, 2696–2700.
- 1033 (85) Schaefer, B. A.; Margulieux, G. W.; Small, B. L.; Chirik, P. J.
1034 Evaluation of Cobalt Complexes Bearing Tridentate Pincer Ligands for
1035 Catalytic C–H Borylation. *Organometallics* **2015**, *34*, 1307–1320.
- 1036 (86) Zhang, L.; Huang, Z. Synthesis of 1,1,1-Tris(boronates) from
1037 Vinylarenes by Co-Catalyzed Dehydrogenative Borylations–Hydro-
1038 boration. *J. Am. Chem. Soc.* **2015**, *137*, 15600–15603.
- 1039 (87) Wen, H.; Zhang, L.; Zhu, S.; Liu, G.; Huang, Z. Stereoselective
1040 Synthesis of Trisubstituted Alkenes via Cobalt-Catalyzed Double
1041 Dehydrogenative Borylations of 1-Alkenes. *ACS Catal.* **2017**, *7*, 6419–
1042 6425.
- 1043 (88) Qiao, L.; Zhang, L.; Liu, G.; Huang, Z. A Highly Efficient Cobalt-
1044 catalyzed Deuteroxygenolysis of Diboron: Synthesis of Deuterated
1045 Pinacolborane and Vinylboronates. *Tetrahedron* **2019**, *75*, 4138–4142.
- 1046 (89) Frisch, M. J.; Trucks, G. W.; Schlegel, H. B.; Scuseria, G. E.;
1047 Robb, M. A.; Cheeseman, J. R.; Scalmani, G.; Barone, V.; Petersson, G.
1048 A.; Nakatsuji, H.; Li, X.; Caricato, M.; Marenich, A. V.; Bloino, J.;
1049 Janesko, B. G.; Gomperts, R.; Mennucci, B.; Hratchian, H. P.; Ortiz, J.
1050 V.; Izmaylov, A. F.; Sonnenberg, J. L.; Williams-Young, D.; Ding, F.;
1051 Lipparini, F.; Egidi, F.; Goings, J.; Peng, B.; Petrone, A.; Henderson, T.;
1052 Ranasinghe, D.; Zakrzewski, V. G.; Gao, J.; Rega, N.; Zheng, G.; Liang,
1053 W.; Hada, M.; Ehara, M.; Toyota, K.; Fukuda, R.; Hasegawa, J.; Ishida,
1054 M.; Nakajima, T.; Honda, Y.; Kitao, O.; Nakai, H.; Vreven, T.;
1055 Throssell, K.; Montgomery, J. A., Jr.; Peralta, J. E.; Ogliaro, F.; Bearpark,
1056 M. J.; Heyd, J. J.; Brothers, E. N.; Kudin, K. N.; Staroverov, V. N.; Keith,
1057 T. A.; Kobayashi, R.; Normand, J.; Raghavachari, K.; Rendell, A. P.;
1058 Burant, J. C.; Iyengar, S. S.; Tomasi, J.; Cossi, M.; Millam, J. M.; Klene,
1059 M.; Adamo, C.; Cammi, R.; Ochterski, J. W.; Martin, R. L.; Morokuma,
1060 K.; Farkas, O.; Foresman, J. B.; Fox, D. J. *Gaussian 16*, revision A.03;
1061 Gaussian, Inc.: Wallingford, CT, 2016.
- 1062 (90) Zhao, Y.; Truhlar, D. G. A New Local Density Functional for
1063 Main-Group Thermochemistry, Transition Metal Bonding, Thermo-
1064 chemical Kinetics, and Noncovalent Interactions. *J. Chem. Phys.* **2006**,
1065 *125*, 194101–194118.
- 1066 (91) Weigend, F.; Ahlrichs, R. Balanced Basis Sets of Split Valence,
1067 Triple Zeta Valence and Quadruple Zeta Valence Quality for H to Rn:
1068 Design and Assessment of Accuracy. *Phys. Chem. Chem. Phys.* **2005**, *7*,
1069 3297–3305.
- 1070 (92) Weigend, F. Accurate Coulomb-Fitting Basis Sets for H to Rn.
1071 *Phys. Chem. Chem. Phys.* **2006**, *8*, 1057–1065.
- 1072 (93) Marenich, A. V.; Cramer, C. J.; Truhlar, D. G. Universal
1073 Solvation Model Based on Solute Electron Density and on a
1074 Continuum Model of the Solvent Defined by the Bulk Dielectric
1075 Constant and Atomic Surface Tensions. *J. Phys. Chem. B* **2009**, *113*,
1076 6378–6396.
- 1077 (94) Hopmann, K. H. How Accurate is DFT for Iridium-Mediated
1078 Chemistry? *Organometallics* **2016**, *35*, 3795–3807.
- 1079 (95) Harvey, J. N.; Himo, F.; Maseras, F.; Perrin, L. Scope and
1080 Challenge of Computational Methods for Studying Mechanism and
1081 Reactivity in Homogeneous Catalysis. *ACS Catal.* **2019**, *9*, 6803–6813.